ESD-TR-67-264

ESD RECORD COPY
RETURN TO
SCIENTIFIC & TECHNICAL INFORMATION DIVISION
(ESTI), BUILDING 1211

ESD ACCESSION LIST
ESTI Call No. AL 56365
Copy No. 1 of 1 cys.

264
COPY

Technical Note 1967-21

M. S. Cohen

Wave Optical Aspects of Lorentz Microscopy

10 May 1967

Prepared under Electronic Systems Division Contract AF 19(628)-5167 by

Lincoln Laboratory

MASSACHUSETTS INSTITUTE OF TECHNOLOGY

Lexington, Massachusetts

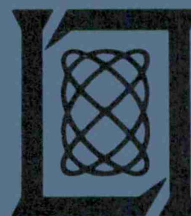

ESLL

AD0652497

The work reported in this document was performed at Lincoln Laboratory, a center for research operated by Massachusetts Institute of Technology, with the support of the U.S. Air Force under Contract AF 19(628)-5167.

This report may be reproduced to satisfy needs of U.S. Government agencies.

Distribution of this document is unlimited.

MASSACHUSETTS INSTITUTE OF TECHNOLOGY
LINCOLN LABORATORY

WAVE OPTICAL ASPECTS OF LORENTZ MICROSCOPY

M. S. COHEN

Group 24

TECHNICAL NOTE 1967-21

10 MAY 1967

LEXINGTON MASSACHUSETTS

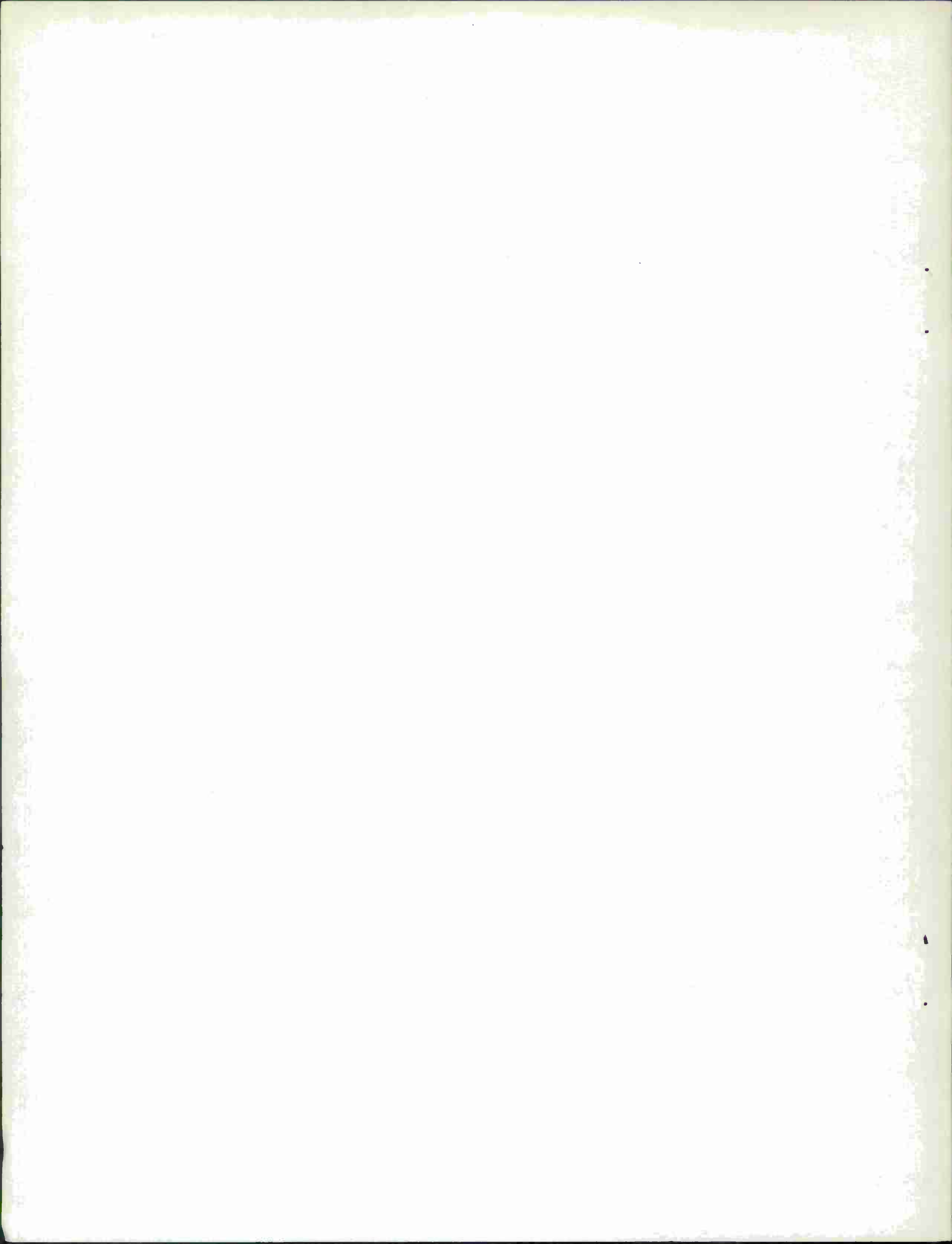

ABSTRACT

The customary defocussed and Foucault modes of Lorentz microscopy are usually described in terms of geometric optics. Wohlleben has shown that geometric optics has a restricted range of validity, however; a more fundamental approach is provided by wave optics. The defocussed and Foucault modes may be discussed in terms of wave optics, and for the defocussed mode it can be shown explicitly that the geometric theory is simply the first approximation to the wave optics theory. Consideration of wave optics also leads to the proposal of two additional modes of Lorentz microscopy: Zernike phase contrast and interference microscopy; these modes cannot be described on the basis of geometric optics. The most fundamental problems in magnetic films which are amenable to study by Lorentz microscopy are investigations of the fine structures of domain walls and magnetization ripple. These problems are discussed in terms of wave optics for all four modes of Lorentz microscopy; in particular the intensity distribution of the zero-width divergent domain wall is explicitly calculated for each mode. For practical experiments the importance of coherence, i.e. of the illumination source size, is emphasized, and the experimental aid of holography is suggested. Since the Wohlleben limit is valid for all four modes, however, there is no resolution advantage inherent in any one mode. The choice of modes for solution of the domain wall and ripple problems therefore depends upon experimental convenience. It is concluded that the defocussed mode seems most promising for practical application; Fresnel diffraction is preferred for the domain wall problem, while Fraunhofer diffraction using low angle electron diffraction techniques will be fruitful for the ripple problem.

Accepted for the Air Force
Franklin C. Hudson, Chief
Air Force Laboratory Office

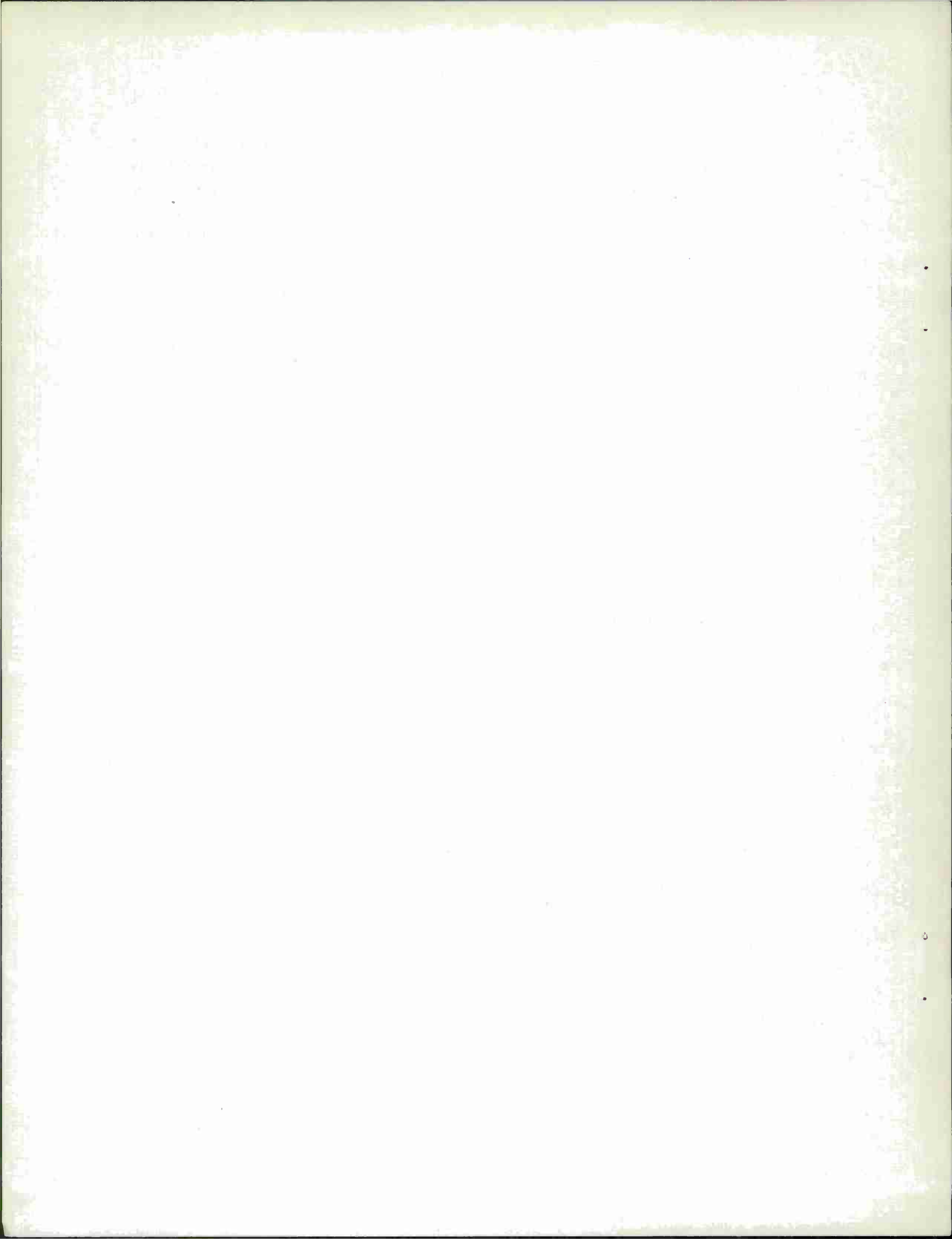

TABLE OF CONTENTS

		Page
I.	INTRODUCTION	1
II.	GEOMETRIC OPTICS THEORY	3
	A. Defocussed Mode	3
	B. Foucault Mode	4
	C. Validity Limit of Geometric Theory	5
III.	WAVE OPTICS THEORY	9
	A. Phase Object	9
	B. Defocussed Mode, Transition from Wave to Geometric Optics	12
IV.	WAVE OPTICS APPLIED TO MAGNETIC FILMS	15
	A. Defocussed Mode	16
	(a) Zero-width Wall	16
	(b) Domain Wall Problem	19
	1. Parametric Method	20
	2. Inversion of the Kirchhoff Integral	22
	(c) Magnetization Ripple Problem	25
	1. Fresnel Diffraction	26
	2. Fraunhofer Diffraction	26
	B. Foucault Mode	28
	(a) Zero-width Wall	28
	(b) Domain Wall and Ripple Problems	30
	C. Zernike Phase Contrast	31
	(a) Zero-width Wall	31
	(b) Domain Wall and Ripple Problems	34
	D. Interference Microscopy	35
	(a) Zero-width Wall	39
	(b) Domain Wall and Ripple Problems	40

V. COHERENCE AND SOURCE SIZE 41

A. Practical Considerations 44

VI. CONCLUSIONS 45

VII. ACKNOWLEDGEMENTS 45

APPENDICES

A-I. KIRCHHOFF DIFFRACTION INTEGRAL 47

A-II. METHOD OF STATIONARY PHASE 50

A-III. HOLOGRAPHY 51

A-IV. KIRCHHOFF DIFFRACTION INTEGRAL FOR RIPPLE 57

A-V. ABBE THEORY OF IMAGE FORMATION BY A LENS 59

A-VI. ZERNIKE PHASE CONTRAST MICROSCOPY 62

REFERENCES 64

I. INTRODUCTION

Lorentz electron microscopy has been used for several years to investigate the magnetic structure of thin ferromagnetic films. In the past, two modes of operation of the electron microscope have been used to obtain Lorentz micrographs, the defocussed and Foucault modes. The mechanisms of contrast formation of these modes have generally been interpreted on the basis of geometric optics.[1,2,3] It has been noted,[4,5] however, that the magnetic structure of a film presents a phase object, not an amplitude object, to the illuminating electron beam and that the fundamental contrast-formation mechanisms should therefore be based on wave optics, not geometric optics. The wave-optical aspect was overlooked by most workers in the field until Wohlleben[6,7] showed that the geometric-optic approach was only an approximation to wave optics, and that this approximation was invalid past a certain limit. Since it is necessary to approach or surpass the geometric optic limit in order to examine the details of magnetic structure in ferromagnetic films, it is necessary to consider wave optics in order to perform high resolution Lorentz microscopy. Consideration of wave optics not only leads to a more basic understanding of the two conventional modes of Lorentz microscopy, but permits the contemplation of completely different modes of electron microscopy for the examination of magnetic structure.

In this report the geometric and wave theories will be reviewed for the two conventional Lorentz modes, and the transition from one theory to the other will be discussed. Several possible experimental arrangements, based on wave optics, are presented for high resolution Lorentz microscope investigation of the two central problems: the fine structure in both domain walls and magnetization ripple.

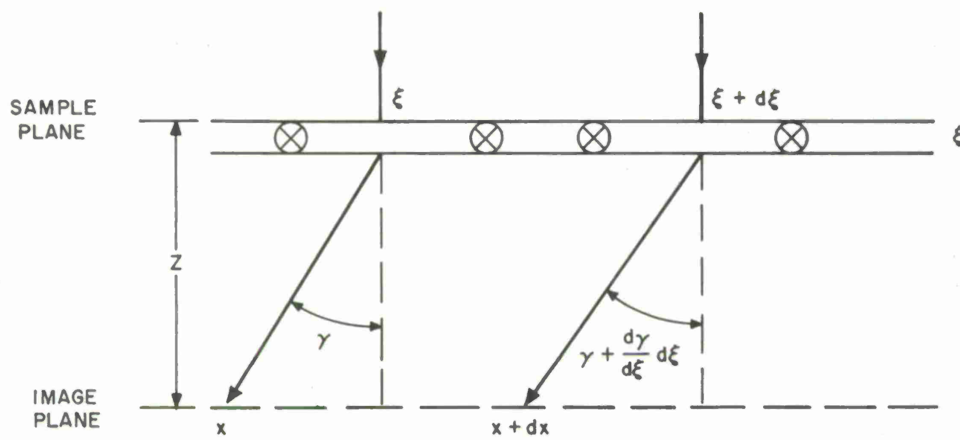

Fig. 1. Ray path for defocussed mode.

II. GEOMETRIC OPTICS THEORY

The geometric theory will now be briefly reviewed[1,2,3] along with Wohlleben's limit of validity of this theory.[6]

A. Defocussed Mode

In this mode, the objective lens of the microscope is focussed on an "image" plane located at a distance Z from the sample plane (Fig. 1).

The relation between the (uniform) intensity I_o in the sample plane to the intensity I(x) in the image plane is desired. It is assumed that the illumination is uniform, parallel, and vertical, and that a ray passing through any point of the sample suffers a deflection γ due to the Lorentz force acting on an electron during its passage through the sample.

For a sample uniformly magnetized in the η direction (perpendicular to the ξ direction), the deflection is

$$(1) \qquad \gamma_o = 4\pi M_o t\left(\frac{e}{2m_e U_e}\right)^{\frac{1}{2}}$$

where t is the sample thickness, m_e the electron mass, M_o the saturation magnetization, and U_e the relativistic accelerating potential. In a non-uniformly magnetized sample, at a point with a magnetization component M_η in the η direction*

$$(2) \qquad \gamma(\xi) = \frac{M_\eta(\xi)\gamma_o}{M_o} .$$

*Throughout this report the magnetization will be considered to be a function of one parameter only, i.e. the problem is assumed to be one-dimensional. Generalization to two-dimensional magnetization distributions should not be difficult.

By conservation of matter, from Fig. 1, $I_o d\xi = I(x)\, dx$ or

$$I_o d\xi = I\{[\xi + d\xi - Z(\gamma + \frac{d\gamma}{d\xi} d\xi)] - [\xi - Z\gamma]\} \quad .$$

Then $\mathcal{I} \equiv I(x)/I_o$ is, using eq. 2,

$$\mathcal{I}(x) = \frac{1}{1 - \frac{Z\gamma_o}{M_o}\left(\frac{dM_\eta(\xi)}{d\xi}\right)} \quad . \tag{3}$$

The relation between a point ξ and its corresponding point x is, from Fig. 1,

$$x = \xi - Z\gamma \quad , \quad \text{or from eq. 2,}$$

$$x = \xi - \frac{Z\gamma_o M_\eta(\xi)}{M_o} \quad . \tag{4}$$

Assuming a given magnetic structure, eqs. 1 through 3 permit the calculation of the intensity $\mathcal{I}(x)$ as a function of x in the image plane, while the image point x is related to the sample point ξ through eq. 4. Note that at focus, i.e. $Z = 0$, there is no contrast, as seen from eq. 3.

B. Foucault Mode

In the Foucault mode, investigated first by Marton[8], the objective lens is focussed on the sample, but an aperture is placed in the back focal plane so as to stop some of the rays from reaching the image plane conjugate to the sample plane.

Consider the sample shown in Fig. 2, i.e. a magnetic film with a zero-width "divergent" domain wall at the optic axis*. Uniform, parallel, horizontal illumination impinges upon the sample from the left. The Lorentz force acting upon the electrons during their passage through the sample causes deflections of $\pm\gamma_o$; hence the rays from the antiparallel domains pass through separate points in the back focal plane. An aperture cutting off half the field in the back focal plane then stops the rays from one domain, but passes the rays from the other, so the first domain appears dark in the image plane while the second appears bright. Thus the intensity is

$$\begin{aligned} &\text{const for } x' > 0 \\ (5) \qquad &0 \quad \text{for } x' < 0 \quad . \end{aligned}$$

C. Validity Limit of Geometric Theory

Wohlleben[6] has shown that there is a fundamental limit to the geometric-optic approach.

First consider the case of a nonmagnetic sample, where Coulomb forces act upon the transmitted electrons. (Specifically a sample consisting of an opaque half-plane abutting a perfectly transparent half-plane may be contemplated). The relation between the uncertainty Δp in the momentum of an electron due to scattering, and the uncertainty $\Delta\xi$ in the position of the associated scattering center in the sample is given by the uncertainty principle:

$$\Delta p_\xi \, \Delta\xi \geq h \quad .$$

When $\Delta p_\xi \, \Delta\xi \sim h$, wave mechanics (wave optics) must be used to find the electron intensity, and diffraction effects are expected, while if $\Delta p_\xi \, \Delta\xi >> h$, classical mechanics (geometric optics) is adequate to solve the problem and no diffraction will be seen. In the present case the value of Δp_ξ is large, of the order of the initial momentum p. Then, since $h/p = \lambda$, $\Delta\xi \geq \lambda$. Thus

*The positive and negative senses of the image plane axis, x', are reversed from those of the sample and focal plane axes, ξ and x, to call attention to the image inversion property of the lens.

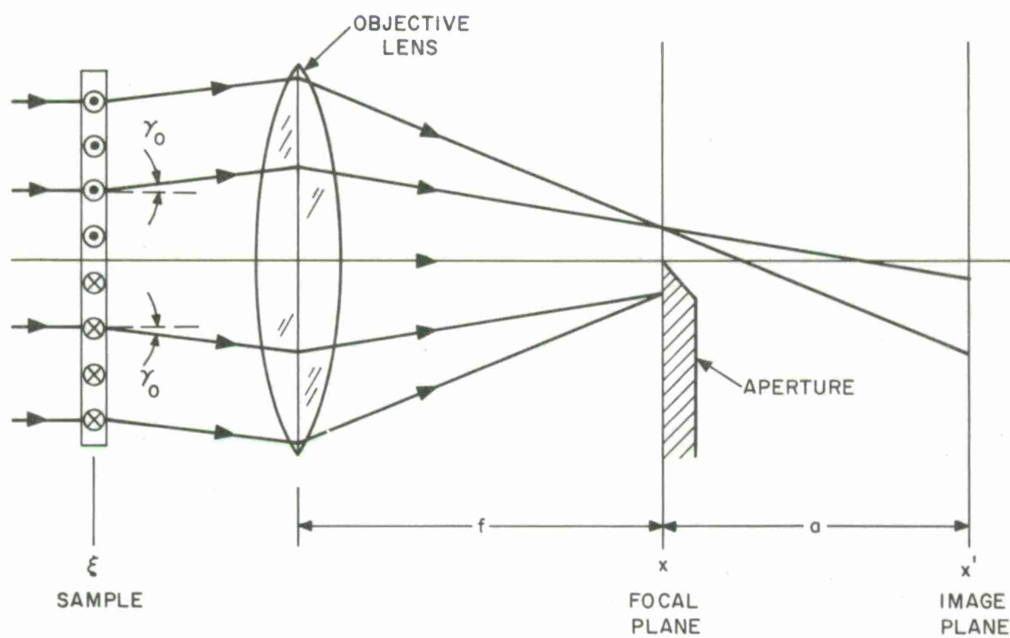

Fig. 2. Foucault mode.

if the electron wavelength is much smaller than the structure it is desired to resolve, geometric optics can be used. The electron wavelength for 100 kv electrons is 0.04Å, which is why structure in the Angstrom range in Coulomb-scattering samples can be resolved by the electron microscope without diffraction effects.

If this analysis held for magnetic scattering samples, magnetic fine structure in magnetic films could easily be resolved without diffraction effects, since that finestructure is in the micron range. The analysis does <u>not</u> hold for the magnetic case, however, essentially because in this case $\Delta p << p$. Consider (Fig. 1) an electron passing vertically through a magnetic sample. Then the horizontally-directed momentum caused by the Lorentz force acting on the electron during passage is $\Delta p_{\xi}(\xi) = [ev\Delta B(\xi)][t/v] = e t \Delta B(\xi)$. Here $B(\xi) = 4\pi M(\xi)$ and v is the electron velocity. Substituting into the uncertainty inequality yields:

$$e\, t\, \Delta B(\xi)\, \Delta\xi \geq h \quad .$$

Thus in the interval $\Delta\xi$, the magnetic induction cannot be determined within an accuracy greater than $\Delta B(\xi)$ as given by this equation. The flux change $\Delta\Phi$ between two ray paths separated by $\Delta\xi$ (Fig. 3) is $\frac{t\,\Delta\xi\,\Delta B}{2}$, so

$$\Delta\Phi \geq \frac{h}{2e} \quad . \qquad (6)$$

Thus, the smallest increment of flux which can be determined classically (geometric optics) is h/2e.

Consider a NiFe film, 500 Å thick, with M = 800 gauss. Then for 1° ripple with a 1 μ period, $\Delta\Phi = 0.13\ h/2e$. Assuming a 2,000Å wide domain wall in this film, at the wall $\Delta\Phi = 4.89\ h/2e$. Thus to obtain high accuracy in the determination of the M distribution, it is necessary to go beyond geometric optics to wave optics.

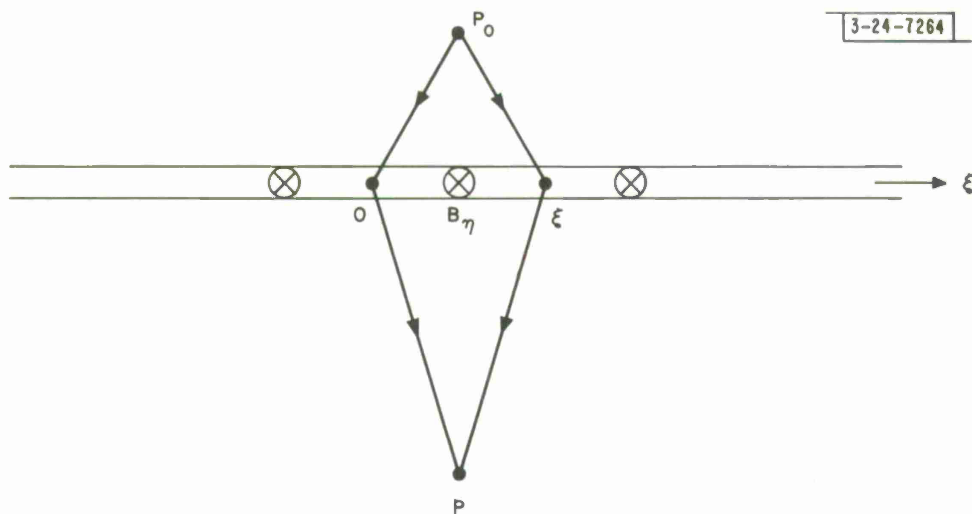

Fig. 3. Illustrating Bohm-Aharonov phase shift.

III. WAVE OPTICS THEORY

A. Phase Object

The key to the wave optical approach is the understanding that magnetic structure in a sample presents a phase object to the electron illumination, i.e. it changes the phase but not the amplitude of the impinging electron waves.[5]

The origin of the phase shift lies in a purely quantum mechanical effect. It was shown by Aharonov and Bohm[9] that the phase difference ϕ between two points P_o and P along an electron ray is given by

$$\phi = -\frac{e}{\hbar} \int_{P_o}^{P} \vec{A} \cdot \vec{dl}$$

where $\vec{A}$ is the vector potential. Then if two rays originate in the same point P_o and end in the same point P, but have different paths between P_o and P, the phase difference between the waves arriving at P is

$$\Delta\phi = -\frac{e}{\hbar}\Big[\underbrace{\int_{P_o}^{P} \vec{A} \cdot \vec{dl}}_{\text{Path 1}} - \underbrace{\int_{P_o}^{P} \vec{A} \cdot \vec{dl}}_{\text{Path 2}}\Big] = -\frac{e}{\hbar} \oint \vec{A} \cdot \vec{dl} = -\frac{e}{\hbar}\Phi$$

where Φ is the total flux enclosed between the two paths.

Now assume (Fig. 3) the sample is a thin magnetic film, of thickness t but infinite in extent, and further assume that there is a variation of the magnetization only in the ξ direction. If one path goes through the origin while the other path goes through point ξ, then

$$\Delta\phi = -\frac{et}{\hbar} \int_{o}^{\xi} B_{\eta}(\zeta)\, d\zeta \tag{7}$$

where $B_\eta = 4\pi M_\eta$ and the η direction is perpendicular to the ξ direction. Then if $P_o O P$ is taken as the reference path, eq. 7 gives the phase shift for any arbitrary path $P_o \xi P$. The object (neglecting the uniform scattering which would occur for a magnetic or nonmagnetic sample) is thus a phase object as stated, with the phase shift $\Delta\phi(\xi)$ given by eq. 7.

If a phase object is examined in focus by a microscope in the manner customary for an amplitude object, no contrast at the observation plane is obtained, but only uniform illumination. Several methods have been developed in light microscopy to provide contrast, i.e. to detect the position-dependent phase shift $\Delta\phi(\xi)$. These methods include the defocussed and Foucault modes discussed above, along with other modes discussed later.

Whichever mode of microscopy is used to examine a magnetic film, the intensity at the image plane can be related to the magnetization distribution in the sample on the basis of wave optics with the aid of eq. 7. For an assumed magnetization distribution in the sample, the results of wave optical calculations for the defocussed and Foucault modes should be much more accurate than the predictions of geometric optics; the latter approach can be viewed as a first approximation to the wave optics theory. For the defocussed mode this statement can be proved for any arbitrary magnetization distribution.

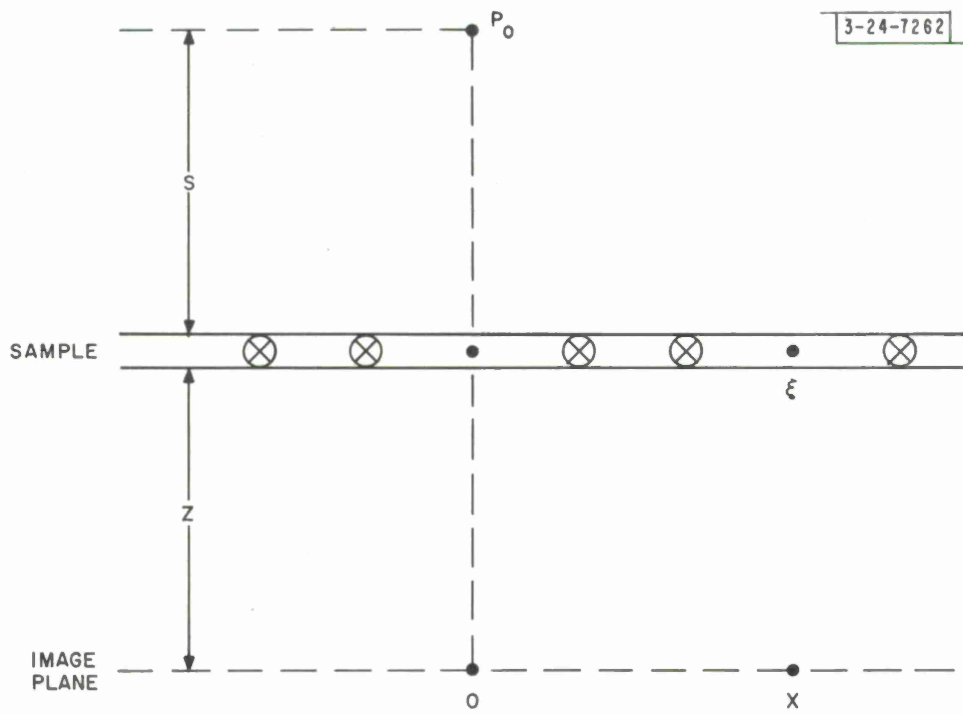

Fig. 4. Defocussed mode by wave optics.

B. Defocussed Mode, Transition from Wave to Geometric Optics

It is desired to find the intensity ratio $\mathcal{J}(x) \equiv I(x)/I_o$ in the defocussed mode (Fig. 4) by wave optics. To do this the excitations of rays $P_o \xi x$ are combined at x in the Fresnel approximation using the Kirchoff diffraction integral[5, 10] (see Appendix A-I) where it is assumed that a ray passing through the sample at point ξ suffers a phase shift given by eq. 7. Then

$$I(x) = \left| A \int_{-\infty}^{\infty} \exp \{ i[\Delta\phi(\xi) + \Omega(\xi)] \} \, d\xi \right|^2 \tag{8}$$

where $\Omega(\xi) = -\frac{kx\xi}{Z} + \frac{k(Z + S)}{2ZS} \xi^2$, A is a constant, and $\Delta\phi$ is given by eq. 7. To find $\mathcal{J}(x)$ note that I_o is determined by substituting $\Delta\phi = 0$ in eq. 8.

To obtain the first approximation to eq. 8, the method of "stationary phase" (Appendix A-II) may be used.[11] Here, assuming $S \gg Z$,

$$f(\xi) = \frac{\Delta\phi(\xi)}{k} - \frac{x\xi}{Z} + \frac{\xi^2}{2Z} \quad . \tag{9}$$

Substitution of $f''(\xi)$ from eq. 9 into eq. A-5 yields, neglecting the factors before the integral

$$I(x) \simeq \frac{2\pi A^2}{\left[\frac{d^2\Delta\phi(\xi)}{d\xi^2}\right]_{\xi=\xi_o} + \frac{k}{Z}} \tag{10}$$

where ξ_o is found from $f'(\xi_o) = 0$ or from eq. 9:

$$\frac{1}{k}\left[\frac{d\Delta\phi(\xi)}{d\xi}\right]_{\xi=\xi_o} - \frac{x}{Z} + \frac{\xi}{Z} = 0 \quad . \tag{11}$$

Substituting eq. 7 into eq. 10, and using the fact (from eq. 10) that $I_o \simeq 2\pi Z A^2/k$,

$$\mathcal{I}(x) \equiv \frac{I(x)}{I_o} = \frac{1}{1 - \frac{4\pi\ Z\ te\lambda}{h}\left(\frac{dM_\eta}{d\xi}\right)} \tag{12}$$

where the relation $k \equiv 2\pi/\lambda$ was used.

Now the wavelength of electrons accelerated to the relativistic potential U_e is

$$\lambda = \frac{h}{(2m_e e\ U_e)^{\frac{1}{2}}} \quad , \quad \text{or from eq. 1}$$

$$\lambda = \frac{h\gamma_o}{4\pi\ M_o te} \quad . \tag{13}$$

Substituting into eq. 12:

$$\mathcal{I}(x) = \frac{1}{1 - \frac{Z\gamma_o}{M_o}\left(\frac{dM_\eta}{d\xi}\right)} \quad , \tag{14}$$

while from eqs. 7, 11, and 13,

$$x = \xi - \frac{Z\gamma_o M_\eta(\xi)}{M_o} \quad . \tag{15}$$

But eqs. 14 and 15 are precisely the relations obtained from geometric optics, eqs. 3 and 4. Thus, the geometric theory is merely the stationary phase approximation to the wave optic theory, while the point x in the image plane corresponding to a given point in the ξ plane is that value of x giving stationary phase for the given ξ.

Consider now the limit of validity of this approximation. Assume that for a <u>given value</u> of x values of ξ in the range $\xi_o - \frac{\Delta\xi}{2} < \xi < \xi_o + \frac{\Delta\xi}{2}$ will contribute appreciably to I(x) in eq. 8 in the stationary phase approximation, while values of ξ outside of the range $\Delta\xi$ will not contribute. Thus, structure <u>within</u> the $\Delta\xi$ range cannot be resolved.

The range of appreciable contribution to the integral $\int_{-\infty}^{\infty} e^{ikf(\xi)}\, d\xi$ is given by $|kf(\xi_o + \frac{\Delta\xi}{2}) - kf(\xi_o)| \leq \frac{\pi}{4}$ since only within this somewhat arbitrary range will constructive interference be expected (Appendix A-II). Expanding $f(\xi_o + \frac{\Delta\xi}{2})$, noting that $f'(\xi_o) \equiv 0$ and substituting from eq. 9, gives for the resolution condition

$$\left| \frac{(\Delta\xi)^2}{8} \left[\left(\frac{d^2\Delta\phi(\xi)}{d\xi^2} \right)_{\xi=\xi_o} + \frac{k}{Z} \right] \right| \geq \frac{\pi}{4} \quad .$$

Now the second term in the inequality represents the uninteresting case of no sample present ($\Delta\phi = 0$). Ignoring it and noting that the first term can be related to the minimum detectable ΔB in $\Delta\xi$ by eq. 7,

$$\Delta\xi \left(\frac{d^2\Delta\phi(\xi)}{d\xi^2} \right)_{\xi=\xi_o} = \frac{2\pi\ te\,\Delta B}{h}$$

, it is seen that

$$\Delta\xi \Delta B\, t \geq h/e \quad , \text{or}$$

$$\Delta\Phi \geq h/2e$$

as found in (eq. 6) from the uncertainty principle.

IV. WAVE OPTICS APPLIED TO MAGNETIC FILMS

The realization that a magnetic film is a phase object, so that possible contrast-formation mechanisms should be discussed on the basis of wave optics, permits more freedom in devising solutions to the two outstanding problems in the magnetic microstructure of films: the details of domain walls and magnetization ripple. Four standard modes of viewing a phase object have been developed in light microscopy: A) Defocussing of the objective lens, B) Foucault, C) Zernike phase-contrast, D) Interference microscopy. The first two modes are the customary modes of Lorentz microscopy; as discussed above they may be described in terms of either geometric optics or wave optics, but the latter approach is more basic and more fruitful (see below). The last two modes may be described only in terms of wave optics. All four modes may be applied to magnetic films.

Each of these modes may, in principle, be completely carried out in the electron microscope. Experimental problems make modes C and D (also B to some extent) difficult, and it may be useful to perform part of the operation in the electron microscope and part outside the microscope using Gabor's holograph technique (Appendix A-III). This technique[12] was first developed for electron microscopy,[13,14] but most of the recent work[12,15] has involved the use of light exclusively rather than electrons and light.

Using Gabor's more practical second method,[14] a photograph is made with the objective lens defocussed from the object; the photograph is known as a hologram. (In this sense all micrographs made with mode A are holograms). If the hologram is suitably illuminated with coherent (laser) light, "reconstructed" radiation appears to originate from an image of the sample at a distance from the hologram equivalent to the defocussing distance. (Actually there is also an unwanted conjugate image, but its influence can be cancelled out with suitable methods[16]). As noted by Gabor et al,[17] all of the standard light optical modes A through D may now be comfortably applied to

the reconstructed radiation.*

Whether a given mode of microscopy is carried out completely in the electron microscope, or partly with the aid of holography, the same analysis on the basis of wave optics should hold. For an arbitrary magnetization distribution it is in general not possible to obtain the intensity distribution in the image plane in closed form, however. On the other hand there is one particularly simple magnetization distribution which is amenable to analytic treatment for each of the four modes. This distribution is that of the zero-width (no internal structure) "divergent" 180° domain wall, used to illustrate the Foucault mode (Fig. 2). Since the consideration of this distribution is instructive, the image plane intensity distribution for each of the four modes of microscopy has been calculated.

In addition to consideration of the zero-width wall, the practicality of each of the four modes for solving the domain wall and magnetization ripple problems will be discussed on the basis of wave optics.

A. Defocussed Mode

(a) Zero-width Wall

To calculate the intensity distribution for the zero-width 180° divergent wall, the Kirchhoff diffraction integral is used (Appendix A-I) in the form of eq. A-3b; with $R(\xi) \equiv e^{i\Delta\phi(\xi)}$:

$$(16) \quad U(x) = A \exp\left[ik(Z+S) + \frac{ikx^2}{2(Z+S)}\right] \int_{-\infty}^{\infty} R(\xi) \exp\left[\frac{ik(Z+S)}{2ZS}\left(\frac{Sx}{Z+S} - \xi\right)^2\right] d\xi \ .$$

For the zero-width wall, $M_\eta = -M_o$ for $\xi > 0$, while $M_\eta = M_o$ for $\xi < 0$. Then

---

*Holography may not be applicable to domain walls, however, because of the large phase shifts associated with them. See Section IV. C-b.

from eq. 7, $\Delta\phi = A_o|\xi|$, where $A_o \equiv \frac{4\pi M_o et}{\hbar}$. Substituting into eq. 16 yields U(x).

This expression can be evaluated in closed form. First, U(x) is written as $U_+(x) + U_-(x)$, where the subscripts refer to the integration ranges $0 < \xi < \infty$ and $-\infty < \xi < 0$, respectively. The transformation $\xi \rightarrow -\xi$ is used to evaluate U_-. Upon completing the square in the integrand, another change of variable permits the expression of U_- and U_+ in terms of Fresnel integrals.[10] The result is, for $x > 0$,

$$U_\pm(x) = A\left(\frac{\pi ZS}{k(Z+S)}\right)^{\frac{1}{2}} \left\{\exp i\left[k(Z+S) + \Theta_\pm\right]\right\} \left\{\left[\tfrac{1}{2} + C(\Sigma_\pm)\right] + i\left[\tfrac{1}{2} + S(\Sigma_\pm)\right]\right\}$$

where

$$\Sigma_\pm \equiv \left(\frac{kSZ}{\pi(Z+S)}\right)^{\frac{1}{2}}\left(\pm\frac{x}{Z} - \frac{A_o}{k}\right) \quad ,$$

and

$$\Theta_\pm = \frac{k}{2Z}\left[x^2 - \frac{SZ^2}{Z+S}\left(\frac{x}{Z} \mp \frac{A_o}{k}\right)^2\right] \quad .$$

Here C and S are the Fresnel integrals, and it is noted[10] that $C(-x) = -C(x)$ and $S(-x) = -S(x)$. Because of the symmetry about the origin, $U(-x) = U(x)$.

The intensity $I = |U_+ + U_-|^2$. It is convenient to normalize to the intensity in the absence of a sample, which is (from eq. 16 for $R(\xi) = 1$) $I_o = \frac{2\pi ZSA^2}{k(Z+S)}$.

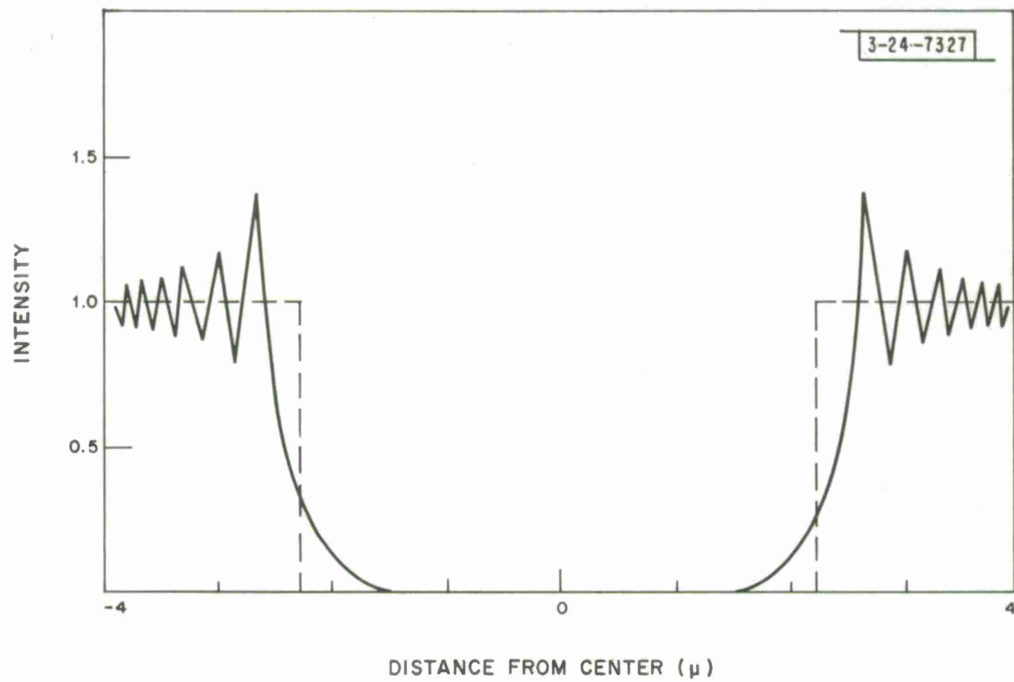

Fig. 5. Relative intensity vs. distance from center of image plane for zero-width divergent 180° wall viewed by the defocussed mode.

By geometric optics all rays for $\xi > 0$ are deflected by an angle γ, while all rays for $\xi < 0$ are deflected by $-\gamma$. Thus at the image plane located a distance Z below the sample the relative intensity I is zero in the range $-\gamma Z < x < \gamma Z$, while I = 1 elsewhere. From the definition of A_o and eq. 13 note that this geometric optical parameter enters the above wave optic equation, since $\frac{A_o}{k} = \gamma$.

Remembering that U_+ and U_- are the contributions for positive and negative ξ respectively, note that for large γZ there will be little contribution of diffracted excitation from the negative ξ to the positive x regions, i.e., U_- can be neglected. Then from the above equation

$$\mathcal{J}(x) \equiv \frac{I(x)}{I_o} \simeq \frac{1}{2}\left\{\left[\frac{1}{2} + C(\Sigma_+)\right]^2 + \left[\frac{1}{2} + S(\Sigma_+)\right]^2\right\} \quad .$$

This is precisely the form for diffraction of radiation[10] from an opaque half plane covering the range $-\infty < \xi < \gamma Z$, with the rest of the ξ plane perfectly transparent.

For 100 kv ($\lambda \sim 0.04$Å), S = 20 cm, Z = 5 cm, the relative intensity was calculated (Fig. 5) for a zero width wall in a 500Å thick film with M_o = 800 gauss. The solid line represents the wave optics prediction while the dotted line is the geometric optics result. The difference in the two results is readily apparent.

(b) Domain Wall Problem

To utilize the defocussed mode for the domain wall and ripple problems, the intensity distribution (found either from a microphotometer trace of a calibrated photographic plate or directly in the microscope with an electron density measurement method[18]) must be matched to the theoretical intensity from the Kirchhoff diffraction integral (eq. 16). The matching process then yields $\Delta\phi(\xi)$ and hence $M_\eta(\xi)$ (eq. 7). Special techniques must be used to make the matching procedure practical.

1. Parametric Method

In calculations of wall energy and shape, Dietze and Thomas[19] assumed a two-parameter Néel wall shape. Later Feldtkeller[20] extended this to a three-parameter shape which permitted the inclusion of the long tail on the wall which was found by Lorentz microscopy[20].

Using the coordinate system shown in Fig. 6, Feldtkeller's assumption may be expressed as

$$\cos\left[\theta(\xi)\right] = \frac{c\left(\frac{\xi}{a}\right)\left[2 + \left(\frac{\xi}{a}\right)^2\right]^{\frac{1}{2}}}{1 + \left(\frac{\xi}{a}\right)^2} + \frac{(1 - c)\left(\frac{\xi}{b}\right)\left[2 + \left(\frac{\xi}{b}\right)^2\right]^{\frac{1}{2}}}{1 + \left(\frac{\xi}{b}\right)^2} .$$

Here the first term gives the shape of the inner structure of the wall, while the second term reproduces the long tail. The parameters a and b are the inner and outer wall widths, respectively, while c is a weighting factor.

From eq. 7

$$\Delta\phi(\xi) = \frac{-4\pi\, e t M_o}{\hbar} \int_0^{\xi} \cos\left[\theta(\zeta)\right] d\zeta . \tag{17}$$

Substituting into the above equation and integrating gives

$$\Delta\phi(\xi) = \frac{-4\pi\, e t M_o a c}{\hbar} \left\{\alpha^{\frac{1}{2}} - 2^{\frac{1}{2}} + \tfrac{1}{2} \ln\left[\left(\frac{\alpha^{\frac{1}{2}} - 1}{2^{\frac{1}{2}} - 1}\right)\left(\frac{2^{\frac{1}{2}} + 1}{\alpha^{\frac{1}{2}} + 1}\right)\right]\right\} \tag{18a}$$

$$- \frac{4\pi\, e t M_o b(1 - c)}{\hbar} \left\{\delta^{\frac{1}{2}} - 2^{\frac{1}{2}} + \tfrac{1}{2} \ln\left[\left(\frac{\delta^{\frac{1}{2}} - 1}{2^{\frac{1}{2}} - 1}\right)\left(\frac{2^{\frac{1}{2}} + 1}{\delta^{\frac{1}{2}} + 1}\right)\right]\right\}$$

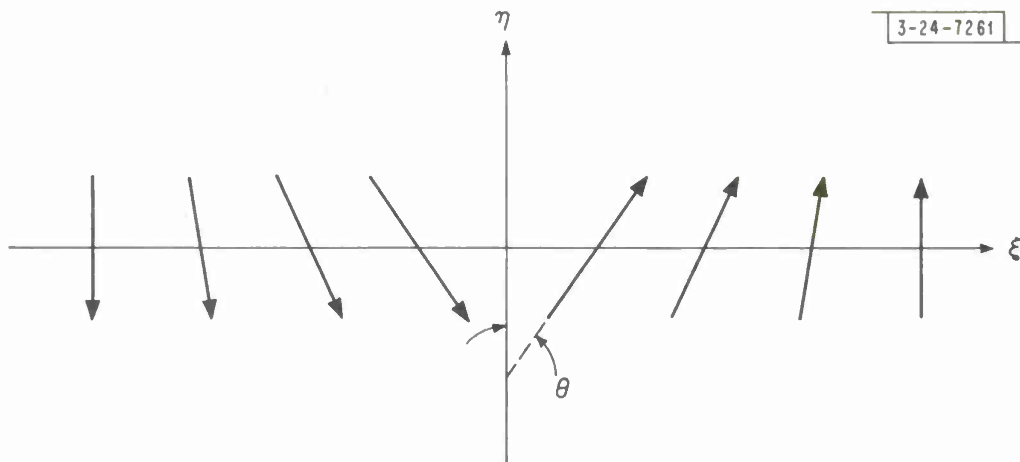

Fig. 6. Model of a Néel wall.

where $\alpha = 2 + (\frac{\xi}{a})^2$ and $\delta = 2 + (\frac{\xi}{b})^2$. Note that as $\xi \to 0$ (wall center),

$\Delta\phi \to 0$; and as $\xi \to \infty$, $\Delta\phi \to \frac{4\pi \ et\ M_o \xi}{\hbar}$ as expected.

The proposed procedure is as follows: Starting from the measured intensity distribution, values of the parameters a, b, and c are first assumed (For a 500 Å Ni Fe film reasonable values are a = 0.1 μ, b = 1.5 μ and c = 0.4 μ). Then $\Delta\phi\ (\xi)$ is found from eq. 18a, and the result is substituted into eq. 8 (with known values of k, Z and S) for a computer calculation of I(x) for an adequate range of points x. The least squares difference from the experimental curve is then found. New values of a, b and c are then assumed and the procedure is repeated. Hopefully the process will converge to give reliable values of a, b and c, thus yielding the wall shape.

Recently Aharoni[21] has calculated that under certain approximations the shape of a Néel wall can be expressed by $\cos [\theta(\xi)] = \tanh (\frac{\xi}{q})$, where the parameter q now has a physical interpretation. Then from eq. 17

(18b) $$\Delta\phi(\xi) = \frac{-4\pi\ et\ M_o q}{\hbar} \ln \cosh(\frac{\xi}{q}) \quad .$$

This one-parameter expression would be easier to apply than eq. 18a.

2. Inversion of the Kirchhoff Integral

There is a more sophisticated way to attack the problem. For an object function $R(\xi) = e^{i\Delta\phi\xi}$ the wave at the image plane is given by eq. 16.

Winthrop and Worthington[22] have shown that this equation can be inverted, i.e. $R(\xi)$ can be expressed in terms of $U(x)$. The solution is

$$(19)\quad R(\xi) = \frac{1}{2\pi A} \exp\left[-ik(Z+S)\right] \int_{-\infty}^{\infty} U(x) \exp\left[-\frac{ikx^2}{2(Z+S)} - \frac{ik(Z+S)}{2ZS}\left(\frac{Sx}{Z+S} - \xi\right)^2\right] dx$$

This can be verified by substituting eq. 19 into eq. 16 and vice versa.

The primary problem is that $U(x)$ is not measured, but only the intensity $|U(x)|^2$, so that only the amplitude and not the phase of $U(x)$ is known. Finding $R(\xi)$ from eq. 19 is thus similar to the problem of determining the structure factor with x rays, where again only intensities and not phases are known.

However, there are techniques* available to obtain the full phase and amplitude information if two different micrographs are taken. Assume that $R(\xi) = e^{i\Delta\phi(\xi)} \simeq 1 + i\Delta\phi(\xi)$. Assume that the diffracted radiation is shifted by $\frac{\pi}{2}$ in phase between micrographs. Such a phase shift is equivalent to replacing $R(\xi)$ by $e^{-i\pi/2} R(\xi)$ in eq. 16. Then from eq. A-10

$$(20)\quad I_{\pm}^2(x) = U_{\pm}(x)\, U_{\pm}^*(x) = \frac{2\pi Z A^2}{k}\left\{1 + \left(\frac{2k}{\pi Z}\right)^{\frac{1}{2}} \int_{-\infty}^{\infty} \Delta\phi(\xi) \cos\left[\frac{\pi}{4} \pm \frac{k}{2Z}(x-\xi)^2\right] d\xi\right\} ,$$

where the plus and minus signs refer to phase shifts of 0 and $-\frac{\pi}{2}$, respectively. From this equation and eq. A-10 it is easily seen that

---

*There may be trouble applying these techniques to domain walls because of the large phase shifts associated with them. See Section IV.C-b.

$$(21) \quad U(x) = A \left(\frac{2\pi Z}{k}\right)^{\frac{1}{2}} \{\exp i[\frac{\pi}{4} + k(Z + S)]\} \left\{1 + \frac{e^{i\pi/4}}{\sqrt{2}} \left[k\left(\frac{I_+(x) + I_-(x)}{4\pi Z A^2}\right) - 1\right] + \frac{k e^{i3\pi/4}}{\sqrt{2}} \left[\frac{I_-(x) - I_+(x)}{4\pi Z A^2}\right]\right\} .$$

This equation can now be substituted into eq. 19 to find $R(\xi)$. To check the procedure, $R(\xi)$ as found from eq. 19 can be substituted into eq. 16 and the result checked against $I_\pm(x)$.

It would be experimentally difficult to introduce a $\frac{\pi}{2}$ phase shift in the diffracted radiation. If holography (Appendix A-III) is used, however, insertion of a quarter wave plate will cause the required phase shift. This technique has been proposed for use in light microscopy by Gabor and Goss.[23]

In another and perhaps easier technique it is again assumed that $R(\xi) \simeq 1 + i\Delta\phi(\xi)$, and in addition that $S \gg Z$. Again two micrographs are taken but without shifting the phase of the illumination. Instead, two different defocussing distances are chosen such that the image planes are equidistant above and below the sample plane. Under these conditions the above two equations hold (in the first equation let $S \to \infty$) if now the plus and minus signs refer to the cases of defocussing below and above the sample, respectively.

Still another approach is to use the parametric form of eq. 18a or 18b with eqs. 16 and 19. The function $R(\xi)$ is first evaluated from $R(\xi) \equiv e^{i\Delta\phi(\xi)}$ for values of the parameters a, b and c which are expected to fit the film being investigated experimentally. Then the function $U(x) \equiv T(x) e^{ig(x)}$ is found from eq. 16, with the values of Z and S used

experimentally. From the experimental intensity trace and the calculated g(x), the function $U'(x) = [I(x)]^{\frac{1}{2}} e^{ig(x)}$ is formed and substituted into eq. 19 to find $R'(\xi)$. From $R'(\xi)$ new values of the parameters a, b and c are found, an improved function $g'(x)$ is constructed from eq. 16 using these new values, and the new function $U''(x) = [I(x)]^{\frac{1}{2}} e^{ig'(x)}$ is used in eq. 19 to give $R''(\xi)$. The process is repeated until the values of the parameters a, b, c or q converge. This procedure should be more practical than the one discussed in the above section "Parametric Method".

(c) Magnetization Ripple Problem

If at any point in the film, $\vec{M}$ is at a local angle θ with respect to the ξ axis, then

$$\vec{M} = [M_o \cos\theta]\,\hat{\xi} + [M_o \sin\theta]\,\hat{\eta} \quad . \tag{22}$$

For one-dimensional magnetization ripple it may be assumed that

$$\theta(\xi) = \int_{-\infty}^{\infty} \theta_\beta \, e^{-i\beta\xi} \, d\beta \tag{23}$$

where β is the wave number of the ripple component, i.e. $\beta = \frac{2\pi}{\rho}$ where ρ is the ripple wavelength. Here $\beta = \frac{n\pi}{Q}$, where n is any positive or negative integer and Q is the width of the film. Further, θ_β is complex, and $\theta_\beta = \theta^*_{-\beta}$ in order to keep θ real. It is the task of Lorentz microscopy to find the ripple spectrum, i.e. $|\theta_\beta|^2$ as a function of β, so that a direct comparison with theory[24] can be made.

Substituting eq. 23 into eq. 22 gives, for small ripple (small $\theta(\xi)$), with the aid of eq. 7:

$$\Delta\phi(\xi) = \frac{i\,4\pi M_o e t}{\hbar} \int_{-\infty}^{\infty} \frac{\theta_\beta}{\beta} \left(1 - e^{-i\beta\xi}\right) d\beta \quad . \tag{24}$$

1. Fresnel Diffraction

Eq. 24 is substituted into eq. 16 to find $I(x)$. A computer procedure, similar to that suggested above for domain walls could be devised where trial functions of the form of eq. 24 would be used in eq. 16. Fortunately, however, in contrast with the domain wall case, $I(x)$ can be found[7] analytically (Appendix A-IV) to an approximation beyond that of geometric optics (eq. A-14). To evaluate θ_β from the experimental intensity distribution $\mathcal{J}(x)$, the latter is Fourier analyzed (Appendix A-IV).

2. Fraunhofer Diffraction

If Z is made large enough, the term involving ξ^2 in eq. 8 may be ignored, giving Fraunhofer diffraction. (Appendix A-I).
Examination of the Fraunhofer diffraction pattern of ripple, rather than the Fresnel diffraction pattern discussed above, is useful because it gives $|\theta_\beta|^2$ as a function of β directly, without the necessity for Fourier analysis of experimental results.

To calculate the Fraunhofer diffraction pattern, it is again assumed that θ is small so that $e^{i\Delta\phi}$ may be approximated as $1 + i\Delta\phi$. Under this assumption, eq. 24 is substituted into eq. 8 where now $\Omega(\xi) = -\frac{kx\xi}{Z}$. This yields, with the aid of the integral representation of the δ function,

$$(25) \quad U(x) = A\left\{\delta(x)\left[1 - \frac{4\pi M_o et}{\hbar}\int_{-\infty}^{\infty}\frac{\theta_\beta}{\beta}\,d\beta\right] + \frac{4\pi M_o et}{\hbar}\int_{-\infty}^{\infty}\frac{\theta_\beta}{\beta}\,\delta\left(\beta + \frac{kx}{Z}\right)d\beta\right\}.$$

The first term is a δ function at the origin from the undiffracted beam. The second term gives the intensity

$$I(x) = C \left(\frac{4\pi M_o et}{\hbar}\right)^2 \left|\frac{\theta_\beta}{\beta}\right|^2 \tag{26}$$

where $\beta = \pm \frac{kx}{Z}$ and C is a constant.

In other words, the distance x in the image plane is directly proportional to the wave number β, while the intensity is proportional to $\left|\frac{\theta_\beta}{\beta}\right|^2$; a scan of I(x) vs x thus leads directly to $|\theta_\beta|^2$ vs β, which may be immediately compared with theory.

Note that if x/Z is expressed as the deflection angle μ, and if $\beta = \frac{2\pi}{\rho}$ while $k = \frac{2\pi}{\lambda}$, from eq. 26: $\lambda = \rho\mu$. This is precisely the Bragg condition for electron diffraction from periodic structure of spacing ρ examined with illumination of wavelength λ. That is, this mode of operation of the microscope is equivalent to finding the electron diffraction pattern of the sample. This may be accomplished in principle by examination of the back focal plane of the objective lens when it is focussed on the sample (Appendix A-V). However, the angles μ involved here are very small (for ρ = 1 micron, λ = 0.04 Å, $\mu = 4 \times 10^{-6}$), so that the techniques of low angle electron diffraction[25] must be used.

The angular divergence α of the undiffracted beam (assumed to be zero in eq. 25) will limit the longest ripple wavelength ρ which can be resolved (Section V). Thus α should be below about 5×10^{-7} radians (smaller than the value usually attained for low angle diffraction) since with this value of α, a ripple wavelength $\rho = \frac{\lambda}{\alpha} = 8\mu$ should be just resolvable. Alternatively if a source of this divergence is used in the Fresnel diffraction method just discussed a coherence length (Section V) of $\frac{\lambda}{\alpha} = 8\mu$ would be attained. Thus the same resolution should be at-

tainable with either method, which is not surprising since the same information is contained in the diffraction pattern at the back focal plane as in the image plane.

Some experiments along these lines have already been carried out[26], but the results were not interpreted in terms of ripple. More recently, electron diffraction from periodic arrays of antiparallel domains in cobalt foils[27,28] has been observed. *

B. Foucault Mode

(a) Zero-width Wall

It is instructive to find, by wave optics, the intensity distribution in the image plane of a lens with an aperture covering half the back focal plane (Fig. 2), for a sample having a single 180° domain wall.[7] Then from eq. 7 and Fig. 2

$$\Delta\phi(\xi) = A_o |\xi| \quad , \quad \text{where } A_o \equiv \frac{4\pi M_o et}{\hbar} \quad . \tag{27}$$

Now by the Abbe theory, the excitation in the image plane is given by a double Fourier transform from the object to the back focal plane then to the image plane. (Appendix A-V). Using $e^{i\Delta\phi}$ (eq. 27) as the object function $R(\xi)$ and using a "filter" function $G(x)$

$$G(x) = 1, \quad x > 0$$
$$= 0, \quad x < 0$$

---

*It may be noted that the intensity distribution from such a square wave magnetization-distribution is not applicable to the present problem which involves sinusoidal magnetization distributions. For the present problem, under the approximation of small $\Delta\phi$ and in the language of ref. 28, the Lorentz peaks fall on the first order interference spots.

(which corresponds to the aperture placed as in Fig. 2), the excitation in the image plane is (eq. A-18):

$$W(x') = C \int_{-\infty}^{\infty} \int_{o}^{\infty} \{ \exp [iA_o |\xi| - \frac{ik}{f} (\xi - \frac{fx'}{D}) x] \} \, dx \, d\xi \quad ,$$

where C is a constant.

This integral may be evaluated explicitly if the upper limit of the x integration is taken _after_ the ξ integration is completed. The result is, for $x' > 0$:

(28)
$$W(x') = \frac{ifC}{k} e^{i A_o fx'/D} \left[Ci \left(\frac{A_o fx'}{D} \right) - i \, Si \left(\frac{A_o fx'}{D} \right) - i \frac{3\pi}{2} \right]$$
$$- \frac{ifC}{k} e^{-i A_o fx'/D} \left[Ci \left(\frac{A_o fx'}{D} \right) + i \, Si \left(\frac{A_o fx'}{D} \right) - \frac{i\pi}{2} \right] \quad .$$

Here[29]

$$Ci(v) \equiv - \int_{v}^{\infty} \frac{\cos t \, dt}{t} \quad \text{and} \quad Si(v) \equiv \int_{o}^{v} \frac{\sin t \, dt}{t} \quad .$$

For $x' < 0$ the above equation holds if $Ci(-v)$ is replaced by $Ci(|v|) + i\pi$, and if $Si(-v)$ is replaced by $-Si(|v|)$.

Eq. 28 gives the wave function in the image plane.* The rapidly oscillating Ci and Si functions originate in diffraction effects; the rapid variations are damped in moving away from the image of the wall (at $x' = 0$). Thus, from eq. 28:

$$\lim_{x' \to \infty} W(x') = \frac{2\pi fC}{k} e^{i A_o fx'/D} \quad ,$$

$$\lim_{x' \to -\infty} W(x') = 0 \quad .$$

---

*For curves of I(x) versus x see ref. 7.

By taking the absolute values, it is seen that the intensity is the same as that found by the geometric theory (eq. 5).

Most of the rapid variation of the Ci and Si functions are over for values of their arguments greater than[29] π. The transition from wave optics to geometric optics can then be said to occur for (eq. 27)

$$\frac{etBfx'}{\hbar D} > \frac{\pi}{2} \quad .$$

This inequality may be generalized[7] by noting that at the domain wall the transition in magnetic induction is $\Delta B = 2B$, while the diffraction-caused transition region in the image plane is $\Delta x' = 2x'$ wide. Then noting that by simple lens theory $\frac{fx'}{D} = \xi$,

$$\frac{t\Delta B\Delta\xi}{2} > \frac{h}{2e}$$

or $\Delta\Phi \geq \frac{h}{2e}$ as found (eq. 6) from the uncertainty principle.

(b) Domain Wall and Ripple Problems

It is difficult to see how this mode can be used to give quantitative magnetization distribution results since the intensity $I(x)$ in the image plane is not proportional to the phase change $\Delta\phi(\xi)$. The method may still be useful for qualitative studies however. Wohlleben[7] has pointed out that $I(x)$ is very sensitive to small changes in the position of the aperture in the back focal plane of the objective lens. The difficulty of positioning the aperture should be obviated if the Foucault mode is carried out with the aid of holography, however (Appendix A-III), because of the magnification of scale associated with the electron to light transition.

C. Zernike Phase Contrast

In this mode (Appendix A-VI) the objective lens is focussed on the sample, while a phase plate made to give a $\frac{\pi}{2}$ phase shift in the focal point region is inserted into the back focal plane. The intensity in the image plane I(x) is then proportional to the phase $\Delta\phi(\xi)$. From eqs 7 and A-22

$$I(x') \simeq C\,[1 - \frac{8\pi et}{\hbar}\int_{0}^{x'/m} M_{\eta}(\zeta)\,d\zeta] \quad ,$$

where $\xi = x'/m$. Thus to find $M_{\eta}(\xi)$ it is necessary only to differentiate the trace of $I(x')$ vs x' at the image plane.

Although Zernike phase contrast microscopy has been performed in the electron microscope[30], the technique is very difficult. The use of holography in conjunction with the microscope should make this mode more practical.

(a) Zero-width Wall

The calculation is again based on the Abbe theory (Appendix A-V), where again $R(\xi) = e^{iA_o|\xi|}$. The presence of a centrally-placed quarter wave plate of radius a at the back focal plane now gives the filter function

$$G(x) = i \quad , \quad -a \leq x \leq a \tag{29}$$

$$= 1 \quad , \quad x < -a, \quad x > a \quad .$$

It is therefore convenient to divide the Abbe integral (eq. A-18) into two parts, W_1 and W_2, where

$$W_1(x') = C\int_{-\infty}^{\infty}\int_{-a}^{a} R(\xi)\,\{\exp\,[-\frac{ik}{f}(\xi - \frac{fx'}{D})\,x]\}\,dx\,d\xi$$

and

$$W_2(x') = C \lim_{L\to\infty} \int_{-\infty}^{\infty} \int_{a}^{L} R(\xi) \{\exp[-\frac{ik}{f}(\xi - \frac{fx'}{D}) x]\} \, dx \, d\xi$$

$$+ C \lim_{L\to\infty} \int_{-\infty}^{\infty} \int_{-L}^{a} R(\xi) \{\exp[-\frac{ik}{f}(\xi - \frac{fx'}{D}) x]\} \, dx \, d\xi \quad .$$

Here C is a constant.

The x integrations may be performed directly. The terms in W_2 involving L and a are then separately collected, from which it can be seen that

$$W_2 = -W_1 + \lim_{a\to\infty} W_1 \quad . \tag{30}$$

It is thus necessary only to evaluate W_1 by completing the ξ integration.

This is easily carried out with an appropriate change of variables. The result, for $x' > 0$, is $W_1 = W_1^+ + W_1^-$, where

$$W_1^{\pm}(x') = \frac{Cf e^{\pm iA_o fx'/D}}{k} \{\pi \pm Si(\Lambda_-) \pm Si(\Lambda_+) + i[Ci(\Lambda_+) - Ci(\Lambda_-)]\} \tag{31}$$

where

$$\Lambda_{\pm} = \frac{kfx'}{D} \left(\frac{a}{f} \pm \frac{A_o}{k}\right) \quad .$$

Note that a/f is the angle subtended at the lens by the edge of the quarter wave plate, while $A_o/k = \gamma$ (see Section IV. A-a) is the geometric Lorentz deflection angle. To obtain the above equation it was necessary to assume that $a/f \geq A_o/k$, i.e. that all the radiation calculated by geometric optics passes well within the area covered by the quarter wave plate. On the wave optic theory, however, all of the radiation does <u>not</u> pass through the quarter wave plate.

Eqs. 29 and 30 yield

$$W = iW_1 - W_1 + \lim_{a\to\infty} W_1, \tag{32}$$

which together with eq. 31 predicts the intensity distribution in the image plane for $x' > 0$. Similar calculations for $x' < 0$ lead to the same equations, but with the signs reversed in the exponent of eq. 31. Note that if eq. 29 were replaced by the condition $G(x) = 1$ for all x, then $W = W_1 + W_2 = \lim_{a\to\infty} W_1$. From eqs. 30 and 31 then

$$W(x') = \frac{Cf}{k} e^{iA_o fx'/D} \quad \text{for } x' > 0, \quad \text{and} \quad W(x') = \frac{Cf}{k} e^{-iA_o fx'/D} \quad \text{for } x' < 0 \quad .$$

The intensity $|W(x')|^2$ would thus be constant in the image plane, and the domain wall would not be visible, as expected directly from the Abbe theory (Appendix A-V).

The presence of the quarter wave plate, however, does not guarantee that phase differences in the sample will be translated directly into intensity differences at the image plane. For this condition to hold it is necessary (Appendix A-VI) that $\Delta\phi(\xi)$ be small enough so that $e^{i\Delta\phi} \sim 1 + i\Delta\phi$. In the present case this means that $A_o \to 0$. However, in order to insure that the diffracted radiation bypasses the quarter wave plate it is also necessary that $a \to 0$, but keeping the condition that $a/f >> A_o/k$.

Under these conditions, to first order in x', $W_1 = \frac{2\pi fC}{k}$, while $\lim_{a\to\infty} W_1 = \frac{2\pi fC}{k}(1 + i A_o fx'/D)$ for $x' > 0$. Then from eq. 32

$$W(x') = \frac{2\pi fC}{k} i(1 + A_o fx'/D) \quad .$$

Since $I = |W|^2$,

(33-a) $$I(x') \propto 1 + 2 \frac{A_o f x'}{D} \quad \text{for } x' > 0 \quad ,$$

while similar considerations show that

(33-b) $$I(x') \propto 1 - 2 \frac{A_o f x'}{D} \quad \text{for } x' < 0 \quad .$$

Eqs. 33 are in direct agreement with the general predictions of the Zernike theory (Appendix A-VI, eq. A-22).

Note that the assumption that $\Delta\phi << 1$ is equivalent to $\frac{A_o f x'}{D} << 1$. It was shown in Section IV. B-a that the geometric optics approximation was valid for the Foucault mode when $\frac{A_o f x'}{D} > \frac{\pi}{2}$. The Zernike case is thus well within the quantum mechanical domain, which is reasonable since this method is based entirely upon wave optics.

(b) Domain Wall and Ripple Problems

The validity condition for the Zernike method applied to a zero-width wall may also be written as $A_o \xi << 1$. For a 500Å film with M_o = 800 gauss, $\xi \lesssim 100$ Å. The Zernike technique (and the holography method, which also assumes $\Delta\phi << 1$) thus seems impractical for domain walls, although it may be applicable to the ripple problem. In that case it would be possible in principle to correlate the ripple structure directly with the crystal structure of the film.

D. Interference Microscopy

In interference microscopy the objective lens forms an image of the sample, while an arrangement is made to bring a reference beam from the illumination source to the image plane by a path avoiding the sample. The interference at the image plane between the reference and transmitted beams creates interference fringes. (Note that this mode differs from those previously discussed; previously interference between rays which all passed through the sample was of importance).

Consider a sample with an arbitrary magnetization distribution $\vec{M}(\xi, \eta)$ in the ξ, η plane, illuminated at vertical incidence with a plane wave. The phase difference between rays passing through points O and P (Fig. 7) can then be found from eq. 7, where it is assumed that the rays through O and P intersect at infinity:

$$\Delta\phi = -\frac{4\pi e t}{\hbar} \int_O^P M_\perp(\zeta)\, d\zeta \quad . \tag{34}$$

Here the integration is taken along the line OP, and $M_\perp(\xi)$ is the magnetization component perpendicular to OP.

The reference beam will interfere with the transmitted beam; the resultant intensity at any point in the image plane conjugate to P will depend upon $\Delta\phi$. If the reference beam is arbitrarily taken to be in phase with the transmitted ray through point O, then intensity extrema (fringes) will be seen when $\Delta\phi = n\pi$, where n is an integer. The fringe spacing is given by eq. 34 when n = 1, which reduces to

$$\Delta\Phi = \frac{h}{2e} \tag{35}$$

where $\Delta\phi$ is the flux change between fringes. The smallest flux change detectable by simply counting fringes is then given by eq. 35 if more accurate knowledge of $M_{\perp}$ between fringes is desired, however, it can be gained by measuring the intensity between fringes. Merely counting the fringes is then, in the Wohlleben limit sense, equivalent to passing to the geometric limit in this mode.

The fringe contours may be calculated using the coordinate system as shown in Fig. 7. Then, from eq. 34

$$n\pi = -\frac{4\pi e t}{\hbar} \int_0^{\ell} \{[\cos \omega]\, M_{\eta}(\zeta) - [\sin \omega]\, M_{\xi}(\zeta)\}\, d\zeta \tag{36}$$

where $\ell = (\xi^2 + \eta^2)^{\frac{1}{2}}$, $\cos \omega = \frac{\xi}{\ell}$ and $\sin \omega = \frac{\eta}{\ell}$.

The transmitted wave directly behind a uniformly magnetized film is given by $\exp(iA_o \xi)$, where $A_o = \frac{4\pi M_o e t}{\hbar}$. This is equivalent to a wave with its wavefront inclined to the horizontal at a small angle ϵ, $\exp(\frac{i2\pi \epsilon \xi}{\lambda})$, under the condition that $\epsilon = \frac{\lambda A_o}{2\pi}$. Maximum intensity fringes would thus appear in the interference microscope when $\frac{\epsilon \xi}{\lambda}$ is an integer, so the fringe spacing $\Delta\xi$ is given by $\frac{\lambda}{\epsilon}$ or

$$\Delta\xi = \frac{2\pi}{A_o} \quad . \tag{37}$$

For a 500Å thick film with M_o = 800 gauss, with λ = 0.04 Å, $\Delta\xi$ = 820 Å, while ϵ = 0.17 minutes.

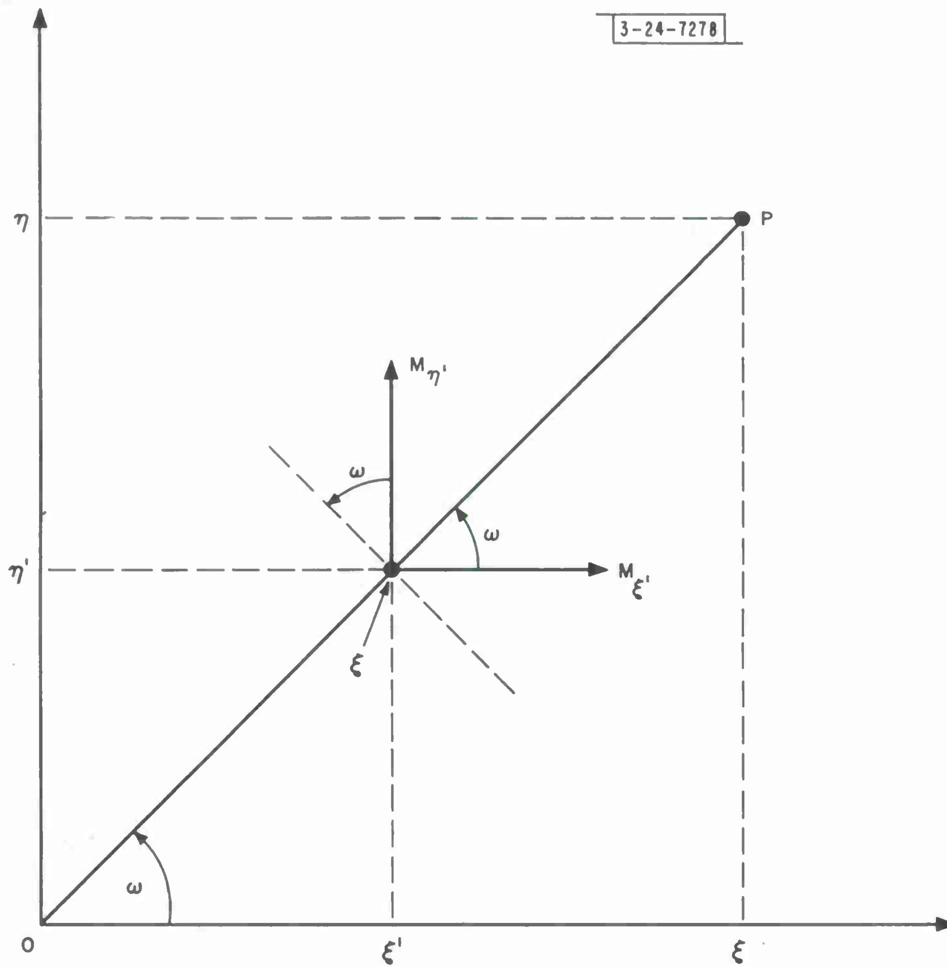

Fig. 7. Coordinate system in sample plane for interference microscopy.

The experimental difficulty is that contrary to the case in light microscopy[10], there is no system whereby a reference electron beam can be superimposed on the transmitted beam while keeping the two wavefronts parallel (in the absence of a sample). It is true that electron microscopes have been modified for use as interference microscopes[31] but the beam superposition is produced by constructing the electron optical analogue of the Fresnel biprism. The transmitted and reference wavefronts are mutually inclined, resulting in a fringe system even with no sample present. This is unsatisfactory for the present application.

A solution to this dilemma is found in the use of holography (Appendix A-III). Here the interference is carried out between the reconstructed light wave passing through the hologram and a reference beam taken from the light source laser. For this purpose[32] the hologram is placed in one arm of an interferometer[33], e.g. a Mach-Zehnder interferometer, and a lens is used so that the real image from the hologram falls on a photographic plate together with the reference beam. The wavefronts of the beams in the two arms are adjusted to be parallel (without the hologram) at the photographic plate.

Equation 37 may be rewritten for this case if ξ is replaced by $\frac{w}{m}$ (Appendix A-III). Following the above equations, the fringe spacing is then

$$\Delta w = m\Delta\xi = \frac{m2\pi}{A_o} \tag{38}$$

while the inclination angle of the wavefront is now $\epsilon' = \frac{\lambda_L \epsilon}{m\lambda}$.

For 4,000 Å light and m = 1,000, for the film discussed above $\Delta w = 82\ \mu$ while $\epsilon' = 17$ minutes. Measurement of fringe spacing of this magnitude and adjustment of parallel wavefronts to well within this angle should be practical with proper instrumentation.

It is possible that a different technique involving holography can be used[34]. Here the sample containing a domain wall is inserted into one of the two beams split by the electron Fresnel biprism in an electron interferometer.[31] A picture is taken. Then the sample is removed (preferably the domain wall is swept out by a magnetic field), and another exposure is made on the same plate. If the developed plate is then treated as a hologram, the reconstructed wavefront will show interference fringes from the superposition of the transmitted beam with and without the sample. In each exposure it is necessary to have the two beams from the Fresnel biprism so that one acts as the inclined reference beam following the customary technique of light holography[15]). The advantage of this method is that careful adjustments of the Mach-Zehnder interferometer are avoided; the disadvantage is that an electron interferometer must be available.

(a) Zero-width Wall

The calculation of the zero-width wall intensity distribution in the image plane is trivial for this mode. It is assumed that the reference beam is of the form $(I_r)^{\frac{1}{2}} e^{ikz}$, while the transmitted beam is of the form $(I_t)^{\frac{1}{2}} e^{i(kz + A_o|\xi|)}$. Then the net intensity is given by

$$I = \left| (I_r)^{\frac{1}{2}} e^{ikZ} + (I_t)^{\frac{1}{2}} e^{i(kZ + A_o|\xi|)} \right|^2$$

or

$$I = I_r + I_t + 2\,(I_r I_t)^{\frac{1}{2}} \cos (A_o|\xi|) \quad .$$

Maximum intensity fringes will thus appear parallel to the wall, separated by the distance $2\pi / A_o$.

(b) Domain Wall and Ripple Problems

The advantage of interference microscopy lies in its ability to translate phase changes in the sample into changes in fringe contours at the image plane, so that intensity measurements do not have to be made. However, since the minimum fringe spacing is at the Wohlleben limit, to investigate the fine structure of a domain wall it <u>would</u> be necessary to make intensity measurements for this mode. Thus there does not seem to be any advantage in employing interference microscopy for the domain wall problem.

The ripple case is even more unfavorable. For 1° ripple, from eq. 37 the fringe spacing would be about 15μ. Since the lateral coherence length is only a few microns (see Section V), there is no hope of investigating ripple with this method.

V. COHERENCE AND SOURCE SIZE

Up to this point it has been assumed that the electron illumination is perfectly coherent, although it is well known that this is far from the case in practical electron microscopy. Since the modes of Lorentz microscopy discussed in Section IV (and the method of holography, Appendix A-III) are based upon diffraction phenomena, the attainable resolution will depend on the degree of coherence of the illumination[35]. To attack the domain wall and ripple problems it is essential that the highest possible degree of coherence be used.

For an electron beam propagating in the Z direction, assume a Gaussian spread of momentum p. Then by the uncertainty principle $\Delta p \Delta Z \sim h$, where ΔZ is the coherence length (i.e. the spatial extent of the wave packet). Then since $p = \hbar k = \frac{h}{\lambda}$ and since the energy $E = p^2/2m$, the coherence length $\Delta Z = \frac{2\lambda}{\Delta U_e / U_e}$ where U_e is the accelerating potential. This is the maximum path difference between two beams, originating from a common source emitting radiation of wavelength λ with energy spread ΔE, for which amplitude interference effects can be sustained. For a 100 kv accelerating potential, $\lambda \sim 0.04$Å; since ΔU_e is usually about 1 volt, $\Delta Z \simeq 8,000$ Å. This is much larger than any possible vertical difference in path lengths discussed above, so the vertical coherence length is not a subject of concern.

The horizontal coherence length is a more serious problem. Assume that the source has a width h and is at a distance S above the image plane, so that it subtends an angle $\alpha = h/S$ at the image plane, (Fig. 8). Then for small α the uncertainty in P_ξ caused by the deviations of the trajectories from the vertical is $\Delta P_\xi = \alpha P$. Since $\Delta P_\xi \Delta \xi \sim h$,

(39) $$\Delta \xi = \frac{\lambda}{\alpha} \quad .$$

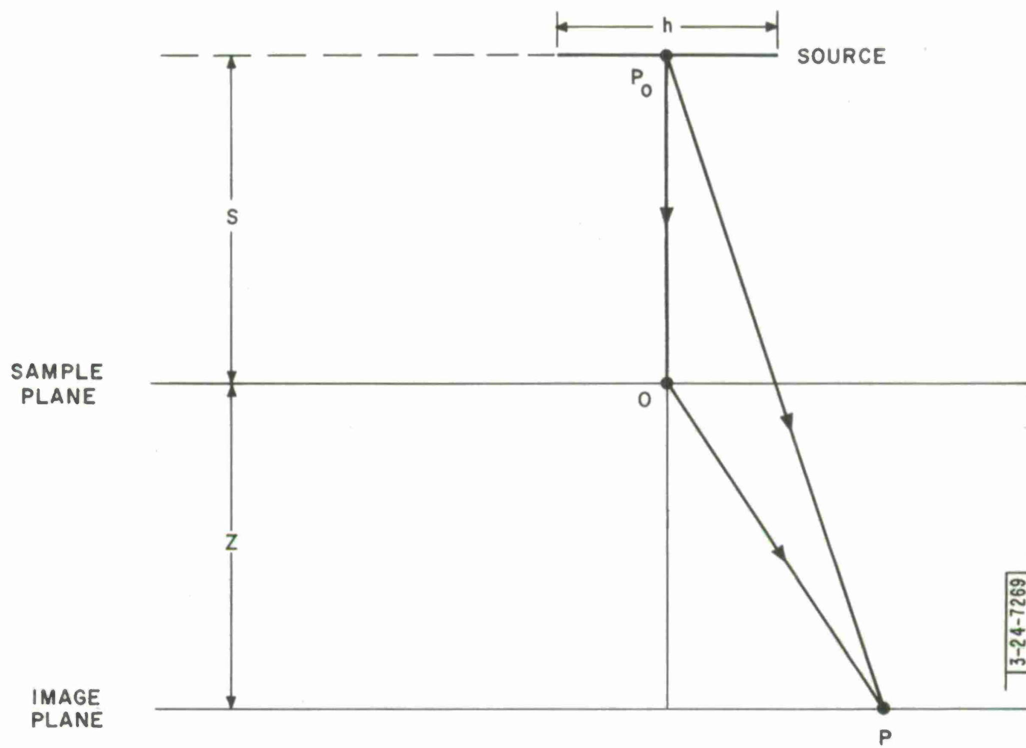

Fig. 8. Illustrating coherence length.

Rays from points in the sample separated by more than $\Delta\xi$ will not interfere coherently. For $\lambda \simeq 0.04\text{Å}$ and for $\alpha \simeq 10^{-5}$, $\Delta\xi = 4,000\text{Å}$. In order to maintain a transverse coherence length greater than the domain wall and ripple structure it is advisable to make $\alpha \sim 10^{-6}$.

Thus in any of the four modes of Lorentz microscopy, magnetic structure on a scale larger than $\Delta\xi$ will not be imaged according to the previous discussions; the image will be either greatly distorted or fully lost. This difficulty is most easily seen in the Fraunhofer diffraction mode (low angle electron diffraction, Section IV. A-c2), with a source of angular divergence α. Rays from long wavelength components ρ diffracted at angles $\mu = \frac{\lambda}{\rho}$ such that $\mu < \alpha$ will be hidden in the undiffracted beam. Thus only components with $\rho < \frac{\lambda}{\alpha}$ will be resolved.

In the defocussed mode, by geometric optics, rays from a broad source which converge through a point in the sample plane will illuminate a circle of diameter αZ in the image plane (Fig. 8). Structure in a region smaller than αZ in size should thus not be resolvable because of overlap from surrounding regions.

The same result may be obtained by wave optics. Consider first the intensity distribution in the image plane from one point of the source at a distance ν from P_o (Fig. 8). For large S and small ν the illumination from this point consists of parallel rays subtending an angle ν/S with the optic axis, so that the phase at any point ξ with respect to 0 is given by $\frac{2\pi\nu\xi}{\lambda S}$. The factor $\exp\left(\frac{i2\pi\nu\xi}{\lambda S}\right)$ should thus be inserted under the integral sign of eq. 16, the integral evaluated and $I = UU^*$ found. Then intensity should then be integrated with respect to ν over the range $-h/2 < \nu < h/2$, and the result divided by h. If this procedure is followed for the ripple case (Appendix A-IV), the additional factor $\left(\frac{\sin\frac{\beta\alpha Z}{2}}{\frac{\beta\alpha Z}{2}}\right)$ appears under the integral sign of eq. A-14.

The contrast thus vanishes unless $\frac{\beta\alpha Z}{2} < \pi$, or ($\beta = \frac{2\pi}{\rho}$) unless $\rho > \alpha Z$, in agreement with the result from geometric optics.

A. Practical Considerations

Now the intensity of illumination j at a point in the object plane is given by $j = b\pi\alpha^2$ for a circularly symmetric source, where b is the source brightness. It is thus seen that the image intensity decreases inversely as $(\Delta\xi)^2$, as α is decreased to increase $\Delta\xi$. A practical point is then reached beyond which α cannot be reduced. Use of three techniques may ameliorate this problem: 1) Pointed filaments have much greater brightness b than ordinary hairpin filaments, and special techniques are available[36] to obtain small source sizes. 2) Many of the problems involved in Lorentz microscopy are essentially one-dimensional. It may thus be possible to use a slit source so that j would be proportional to α, not α^2. 3) Use of modern image intensifiers may make patterns visible at very low illumination levels. It must be noted, however, that even when α is vanishingly small there will still be an effective α because of inelastic scattering in the sample.

Precautions must also be taken to ensure that the focal length of the lenses do not change because of accelerating potential or lens current fluctuations, and that rapidly-varying stray fields[37] or mechanical vibrations do not blur the patterns formed on the photographic plate during the necessarily long exposure time.

VI. CONCLUSIONS

It has been demonstrated that the basic wave optical approach is very fruitful for a fuller understanding of the defocussed and Foucault modes, and that it leads to consideration of the Zernike phase contrast and interference microscopy modes. It has been shown that it is necessary to take account of diffraction effects in each mode, i.e., the Wohlleben limit is valid for all four modes so that there is no resolution advantage inherent in any one mode. The choice of mode for investigation of the domain wall and ripple problems will therefore depend primarily on experimental convenience. At this point it would appear that the defocussed mode will be most useful for both problems; Fresnel diffraction is preferred for the domain wall problem, while Fraunhofer diffraction will be a powerful technique for the ripple problem. In any case all of these techniques face the same fundamental coherence limitation to the resolution; this central problem of the illumination source must be solved before quantitative results can be obtained. The experimental complications in many of these modes can be reduced with the aid of the holographic technique.

VII. ACKNOWLEDGEMENTS

D. Wohlleben, D. O. Smith, and K. J. Harte are thanked for helpful discussions. The use of holography as an aid to Lorentz microscopy was first proposed by D. O. Smith.

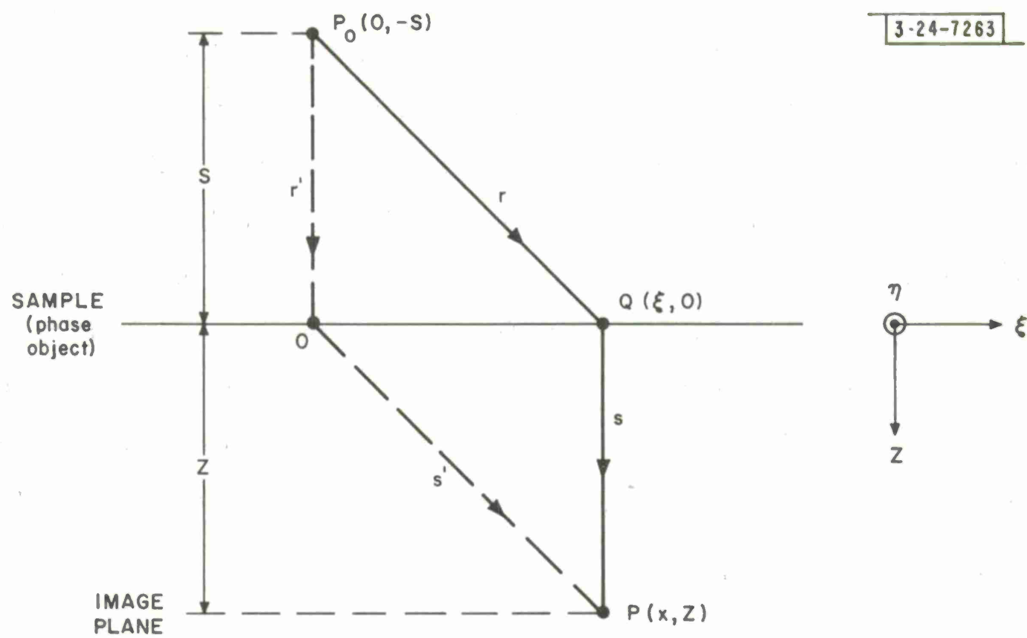

Fig. A-1. Illustrating Kirchhoff diffraction integral.

APPENDICES

A-I. KIRCHHOFF DIFFRACTION INTEGRAL

The Kirchhoff diffraction integral gives the amplitude of the radiation, U, at any image point P(x,Z) when a phase object is interposed between the illumination source P_o(O, -S) and P (Fig. A-1). The phase object shifts the phase of any ray passing through point Q(ξ, 0) of the object by $\phi(\xi)$. The problem has been particularized to two dimensions in Fig. A-1. Here the origin is taken at point O in the object, while the x and Z directions are assumed to be horizontal and vertical, respectively.

Assuming the distances r and s are large compared with the extent of the object, the Kirchhoff diffraction integral[10] gives the amplitude at P:

$$U = \text{const} \int_{-\infty}^{\infty} e^{i\phi(\xi)} e^{ik(r+s)} d\xi \qquad \text{(A-1)}$$

where $k = 2\pi/\lambda$ and λ is the wavelength of the illuminating radiation. Thus in eq. A-1 to find U the excitations at P from all rays P_oQP are added, for all points Q in the range $-\infty < \xi < \infty$. In this addition attention is paid to the phase differences of each excitation, whether such differences be caused by different path lengths r + s or different phase shifts ϕ on passage through different points Q of the object.

Consider the reference path P_oOP with the object phase shift ϕ_o. Then if

$$\Delta\phi(\xi) \equiv \phi(\xi) - \phi_o$$

eq. A-1 can be rewritten

$$\text{(A-2)} \quad U = Ae^{ik(r'+s')} \int_{-\infty}^{\infty} e^{i\Delta\phi(\xi)} \, e^{ik[(r-r') + (s-s')]} \, d\xi$$

where, realizing that eventually only $|U|^2$ is of interest, $e^{i\phi_o}$ is absorbed into the constant A.

By geometry

$$r^2 = \xi^2 + S^2 \qquad s^2 = (x-\xi)^2 + Z^2$$

$$(r')^2 = S^2 \qquad (s')^2 = x^2 + Z^2$$

Expressing, by the abcve equations, r in terms of r' and s in terms of s' and expanding,

$$r - r' = \xi^2/2r' + \ldots$$

$$s - s' = -\frac{x\xi}{s'} + \frac{\xi^2}{2s'} + \ldots$$

Note that

$$r' = S$$

and

$$s' = (Z^2 + x^2)^{\frac{1}{2}} = Z + \frac{x^2}{2Z} + \ldots$$

Keeping only the initial terms of the above four equations yields upon substitution into eq. A-2:

$$\text{(A-3a)} \qquad U(x) = Ae^{ik[(Z+S) + x^2/2Z]} \int_{-\infty}^{\infty} R(\xi) \, e^{i\Omega(\xi)} \, d\xi$$

where

$$\Omega(\xi) = -\frac{kx\xi}{Z} + \frac{k(Z+S)\,\xi^2}{2ZS} \quad , \quad A \text{ is a constant,}$$

and

$$R(\xi) = e^{i\Delta\phi(\xi)} \quad .$$

Alternatively this equation may be written as

(A-3b) $$U(x) = Ae^{ik\left[(Z+S) + \frac{x^2}{2(Z+S)}\right]} \int_{-\infty}^{\infty} R(\xi)\exp\left[i\frac{k(Z+S)}{2ZS}\left(\frac{Sx}{Z+S} - \xi\right)^2\right]d\xi \quad .$$

Often the approximation $S \gg Z$ can be made in eqs. A-3a and A-3b).

If the extent of the sample is small compared with Z, then the ξ^2 term may be neglected in eq. A-3 . This case is called Franhofer diffraction. If both terms in ξ must be considered the result is known as Fresnel diffraction.

A-II. METHOD OF STATIONARY PHASE[11]

The following is a heuristic presentation of the method; for more details see Jeffries and Jeffries.[11]

Consider the integral

$$J = \int_{-\infty}^{\infty} e^{ikf(u)} du \quad . \tag{A-4}$$

Expand $f(u)$:

$$f(u) = f(u_o) + uf'(u_o) + \frac{u^2}{2} f''(u_o) + \ldots \quad .$$

It is seen that, upon substituting this equation into eq. A-4, the plane waves $e^{ikf'(u_o)u}$ will destructively interfere in general, so that all contributions to J will vanish. At the value u_o where $f'(u_o) = 0$, however, it is possible to have nonzero contributions to J. Then keeping only the first three terms of the series:

$$J \simeq e^{ikf(u_o)} \int_{-\infty}^{\infty} e^{ikf''(u_o)\, u^2/2}\, du \quad .$$

Let $\frac{\pi}{2}\, r^2 = \frac{kf''(u_o)\, u^2}{2}$, and express the integrand in terms of sin and cos. The integral is then expressed in terms of known Fresnel integrals[10], and

$$J \simeq \left[\frac{2\pi}{kf''(u_o)} \right]^{\frac{1}{2}} e^{i\pi/4}\, e^{ikf(u_o)} \tag{A-5}$$

where u_o is found from

$$f'(u_o) = 0 \quad . \tag{A-6}$$

A-III. HOLOGRAPHY

Holography[12,15] can be considered as a process in which radiation from an object is "frozen" at a plane in space in such a way that the radiation can be later "unfrozen" and allowed to continue on to the observer. The freezing process is merely exposure of a photographic plate, called a hologram, at the plane in question; unfreezing is accomplished by re-illumination of the hologram. In order for this method to work the original radiation and that used for reconstruction must be coherent, although their wavelengths may differ. Further, strong uniform background radiation must accompany the radiation from the object during the exposure of the hologram.

In electron microscopy[14], the hologram is formed by taking a micrograph with the objective lens focussed on an image plane at a distance Z from the sample (Fig. 1). Reconstruction is carried out with coherent (laser) light.

To discuss holography quantitatively, the exposure process of photographic plates must first be considered. If a photographic plate is illuminated with radiation of amplitude U for a time τ then the density D of that plate is (in its "linear" region):

$$D = \Gamma \ln (|U|^2 \tau)$$

where Γ is a constant. Here $D = \ln(t^{-2})$ where t is the amplitude transmission of the plate to light after exposure. Substituting, $t_n = (K_n|U|)^{-\Gamma_n}$ is the transmission of the negative. In the printing of the positive from the negative the exposure is proportional to t_n, so

$$t_p = \left[K_p(K_n|U|^{-\Gamma_n}\right]^{-\Gamma_p} = K|U|^{\Gamma} \qquad \text{(A-7)}$$

where $\Gamma = \Gamma_n \Gamma_p$ is the net gamma.

The excitation at the image plane for a phase object is given by eq. A-3a. In order to ensure a strong background wave the perturbation on the illumination by the sample is kept small (e.g. a very thin sample is used) so that $e^{i\Delta\phi}$ may be approximated as $1 + i\Delta\phi$, giving

$$\text{(A-8)} \qquad U(x) = A\, e^{ik(Z + S + x^2/2Z)} \left[\int_{-\infty}^{\infty} e^{i\Omega(\xi)} d\xi + i \int_{-\infty}^{\infty} \Delta\phi(\xi)\, e^{i\Omega(\xi)} d\xi \right] .$$

The first integral may be found by first completing the square in $\Omega(\xi)$, then by evaluation in terms of Fresnel integrals.[10] The result is

$$\text{(A-9)} \qquad \int_{-\infty}^{\infty} e^{i\Omega(\xi)} d\xi = \left[\frac{2\pi ZS}{k(Z+S)} \right]^{\frac{1}{2}} e^{i\pi/4} \exp\left[- \frac{ikSx^2}{2Z\,(Z+S)} \right] .$$

Assuming $S >> Z$ in eq. A-9, eq. A-8 may be rewritten

$$\text{(A-10)} \; U(x) = A\left(\frac{2\pi Z}{k}\right)^{\frac{1}{2}} e^{i\pi/4}\, e^{ik(Z+S)} \left\{ 1 + i\left(\frac{k}{2\pi Z}\right)^{\frac{1}{2}} e^{-i\pi/4}\, e^{i\frac{kx^2}{2Z}} \int_{-\infty}^{\infty} \Delta\phi(\xi)\, e^{i\Omega(\xi, x)} d\xi \right\} .$$

The term outside the braces in eq. A-10 is simply proportional to the direct wave from the source to the image plane of Fig. A-1; this amplitude is modified by the weak wave, originating in the phase object, expressed by the second term in the braces.

The electron microscope permits the image given by eq. A-10, magnified m times by the lens system, to expose a photographic plate and thus to create a hologram. The amplitude transmission t(w) of the hologram is then obtained by finding $| U(\frac{w}{m})| = [U(\frac{w}{m})\, U^*(\frac{w}{m})]$ from eq. A-10 (where $w = mx$ is the coordinate measured on the hologram), substituting into eq. A-7 and expanding to first order.

In the reconstruction process the hologram is illuminated by a wave $U_R = R\, e^{ik_L(S_L + Z_L)}$, of wave number $k_L = 2\pi/\lambda_L$, originating from a point

$S_L + Z_L$ from the hologram. The excitation just behind the hologram is then, letting C be a constant,

$$(A\text{-}11) \qquad U_S(w) = U_R t(w) = C e^{ik_L(S_L + Z_L)} \Big\{ 1 +$$

$$\frac{i\Gamma}{2}\left(\frac{k}{2\pi Z}\right)^{\frac{1}{2}} e^{-i\pi/4}\, e^{i\frac{kw^2}{2m^2 Z}} \int_{-\infty}^{\infty} \Delta\phi(\xi)\, e^{i\Omega(\xi, w/m)}\, d\xi$$

$$- \frac{i\Gamma}{2}\left(\frac{k}{2\pi Z}\right)^{\frac{1}{2}} e^{i\pi/4}\, e^{-i\frac{kw^2}{2m^2 Z}} \int_{-\infty}^{\infty} \Delta\phi(\xi)\, e^{-i\Omega(\xi, w/m)}\, d\xi \Big\} \quad .$$

Under certain conditions it may be concluded, by comparing eqs. A-10 and A-11, that holography is successful here, i.e. that $U_S(w) = U(x)$. That is, the excitation just behind the hologram (and hence at all distances below it) is the same as that caused by a virtual image of the sample, magnified m times, placed a distance Z_L above the hologram. These conditions are that $\Gamma = 2$ (deviations from 2 are unimportant, however), the exponential factors before the braces in eqs. A-10 and A-11 are equal in magnitude (see below), and that the last term in the braces is ignored. This last term represents a real image of the sample, magnified m times, at a distance Z_L below the hologram. Either the real or virtual reconstructed images may be examined by the viewer, but the radiation from the other conjugate image will be experienced as background noise.

The magnitude of the exponential factor before the braces in eq. A-11 will be correct if, in the reproduction process, the distance from light source to hologram is scaled according to the light/electron wavelength ratio:

$$(A\text{-}12) \qquad S_L + Z_L = \frac{\lambda_L}{\lambda}(S + Z) \quad .$$

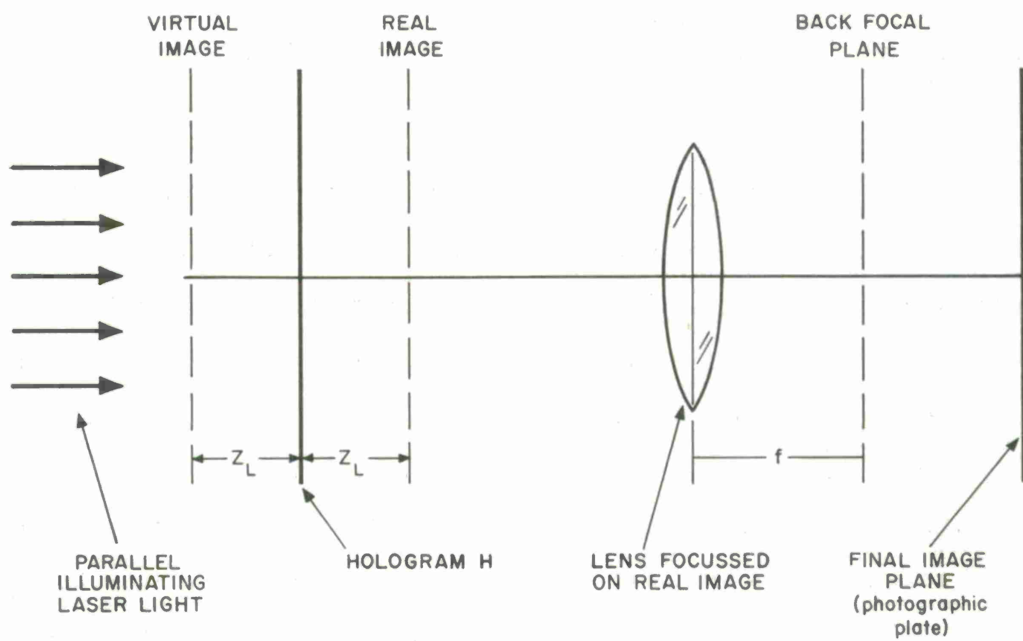

Fig. A-2. Illustrating holographic reconstruction.

Here the subscript L denotes values used in reconstruction (light); no subscript means values used in the production of the hologram (electrons).

The distance Z_L may be found by considering the production of a hologram using light of wavelength λ_L (wavenumber k_L) illuminating a sample of coordinate w with distances S_L and Z_L; these symbols are substituted into eq. A-10 and w replaces x while ξ_L replaces ξ. The resulting U(w) must be the same as $U_S(w)$ from eq. A-11. For this to be true the magnitude of the exponentials before the integrals must be the same, or

$$\frac{k_L w^2}{2Z_L} = \frac{kw^2}{2m^2 Z} \quad , \quad \text{or}$$

$$Z_L = \frac{m^2 \lambda Z}{\lambda_L} \quad . \tag{A-13}$$

It is also necessary that $\xi_L = m\xi$, so that the image formed by the hologram reconstruction is magnified m times the sample size (under the assumption of plane waves for illumination and reconstruction).

Typical values are $m = 10^3$, $\lambda = 0.04$ Å, $\lambda_L = 4{,}000$ Å, S = 20 cm, Z = 1 cm. From eq. A-12, $S_L + Z_L = 2.1 \times 10^5$ cm, i.e., in the reconstruction process parallel laser light may be used. The defocus distance Z_L is 10 cm.

The holographic reconstruction apparatus is shown in Fig. A-2 rotated to a horizontal position. The light to the right side of the hologram H appears to come both from the virtual image at Z_L to the left of H and the real image Z_L to the right of H. The various methods for rendering phase objects visible may now be used. For example, a lens may be focussed on the real object while either a Foucault stop or Zernike quarter wave plate is placed in its back focal plane. This would give visible contrast at the image plane of the lens, where a photographic plate may be placed.

The unwanted virtual object gives an undesired background at this image plane. Now, when light is used both for the hologram recording and reconstruction, in contrast with the Gabor in-line method described here, reference radiation coincident with the object radiation is not usually used.[15] Instead, it is customary to use reference radiation impinging on the hologram at an angle from the radiation coming from the sample, which causes a spatial separation of the real and ghost images at reconstruction. This technique is impractical for electron microscopy, however. On the other hand, a suggestion by Bragg and Rogers[16] may be useful. Since the lens in Fig. A-2 is focussed on the real image at Z_L to the right of H, the photographic plate records the real image and a hologram of the virtual image made at a defocus distance $2Z_L$. Suppose a hologram is made in the microscope at a defocus distance 2Z, and is printed as a negative. If this hologram is placed at the object plane of the lens, which coincides with the real image, the radiation from the virtual image will be cancelled out. More practically a photographic plate could first be exposed with the apparatus of Fig. A-2 without the negative hologram, but with the hologram H. Then another plate could be exposed without H but with the negative hologram made at 2Z. The two plates could then be superimposed and a positive print made; this print would contain the real image only.

A-IV. KIRCHHOFF DIFFRACTION INTEGRAL FOR RIPPLE

The result of the substitution of eq. 24 into eq. 8 is to be evaluated explicitly. To do this assume that θ is small so that the factor $e^{i\Delta\phi}$ may be approximated as $1 + i\Delta\phi$. The result is $I(x) = |U(x)|^2$, where $U(x)$ is given by eq. A-8. The first term in eq. A-8 is given by eq. A-9; to evaluate the second term it is necessary only to note, upon substitution of eq. 24, that it contains integrals of the form of the first term but with x replaced by $x + \frac{Z\beta}{k}$. Then, assuming that $S >> Z$,

$$\mathcal{J}(x) \equiv \frac{I(x)}{I_o} \cong \left| 1 + \frac{4\pi M_o e t}{\hbar} \int_{-\infty}^{\infty} \frac{\theta_\beta}{\beta} \exp\left[-i(\beta x + \frac{Z\beta^2}{2k})\right] d\beta \right|^2 .$$

The absolute value is found to first order, giving with the use of the fact that $\theta_\beta = \theta^*_{-\beta}$

$$\text{(A-14)} \qquad \mathcal{J}(x) \simeq 1 - \frac{i8\pi M_o e t}{\hbar} \int_{-\infty}^{\infty} \frac{\theta_\beta}{\beta} \sin\left(\frac{Z\beta^2}{2k}\right) e^{-i\beta x} d\beta \quad .$$

This result may be compared with that obtained from the geometric theory. Substituting eq. 23 into eq. 22 gives, for small θ, upon substitution into eq. 3

$$\mathcal{J}(x) = \frac{1}{1 + iZ\gamma_o \int_{-\infty}^{\infty} \beta\theta_\beta \, e^{-i\beta\xi} \, d\beta} \quad .$$

Expanding and using eq. 13

$$\text{(A-15)} \qquad \mathcal{J}(x) \cong 1 - \frac{i4\pi M_o e t Z}{\hbar k} \int_{-\infty}^{\infty} \beta\theta_\beta \, e^{-i\beta\xi} \, d\beta \quad .$$

From an examination of eq A-14 it is seen that as the ripple wavelength becomes much larger than the electron wavelength ($\lambda << \rho$) the geometric expression eq. A-15 is approached. Further, it is seen that wave optical effects can cause values of I(x) significantly different from those predicted from geometric optics.

To find θ_β as a function of β from the experimental intensity distribution I(x), the inverse Fourier transform of eq. A-14 is taken, yielding

$$Re(\theta_\beta) = \frac{\beta}{2\pi \sin(\frac{Z\beta^2}{2k})} \int_{-\infty}^{\infty} Y(x) \sin\beta(x) \, dx$$

and

$$Im(\theta_\beta) = \frac{-\beta}{2\pi \sin(\frac{Z\beta^2}{2k})} \int_{-\infty}^{\infty} Y(x) \cos\beta(x) \, dx$$

where

$$Y(x) \equiv \frac{\hbar [1 - \mathcal{J}(x)]}{8\pi M_o e t} \quad ,$$

which give the real and imaginary parts of θ_β, respectively. Once the experimental intensity traces have been Fourier analyzed, the values of θ_β as a function of θ obtained with the aid of the above equations may be compared with theory[24], which predicts $|\theta_\beta|^2$ as a function of β.

A-V. ABBE THEORY OF IMAGE FORMATION[10] BY A LENS

The Abbe theory states that the wave function at the back focal plane of a lens is the Fourier transform of the wave function at the object, while the wave function at the image plane is the Fourier transform of the wave function at the back focal plane.

The wave function at the back focal plane of a lens focussed on an object (Fig. A-3), is given by eq. A-3a with the general object function $R(\xi)$ replacing $e^{i\Delta\phi}$. This excitation is equivalent to that for no lens as $Z \to \infty$; so the second term in $\Omega(\xi)$ vanishes (also assuming $S >> Z$).

The first term in $\Omega(\xi)$ may be alternatively written as $k\xi \tan\theta$, where $\theta \equiv \tan^{-1}\frac{x}{z}$ is the angle of the ray emerging from the object (Fig. A-1). With a lens interposed between the object and the image plane, all rays leaving the object at the angle θ will be focussed at the same point x in the focal plane where $x = f \tan\theta$ (Fig. A-3). Then x/Z in eq. A-3a should be replaced by x/f for this configuration. The excitation in the focal plane is then given by

$$V(x) = C_1 \int_{-\infty}^{\infty} R(\xi)\, e^{-ikx\xi/f}\, d\xi \qquad \text{(A-16)}$$

which represents Fraunhofer diffraction.

The excitation at the image plane may be found by applying eq. A-3 again, considering Fraunhofer diffraction from the focal plane to the image plane. The sign of the exponent is now changed, while in compensation, positive and negative senses of the x' axis are reversed from those of the x axis. (This procedure calls attention to the image inversion property of the lens). Then

$$W(x') = C_2 \int_{-\infty}^{\infty} G(x)\, V(x)\, e^{i\frac{kx'x}{D}}\, dx \quad . \qquad \text{(A-17)}$$

Here $G(x)$ is a "filter function" which describes the action of a physical

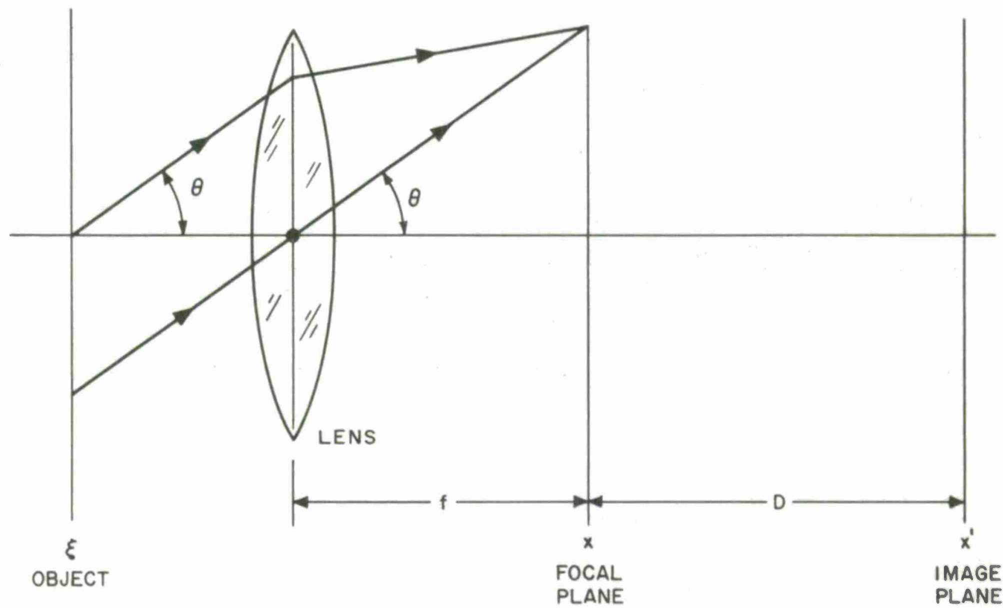

Fig. A-3. Illustrating Abbe theory of image formation by a lens.

filter or stop placed at the focal plane, and C_1 and C_2 are constants.

Substituting eq. A-16 into A-17 and reversing the order of integration,

$$W(x') = C_1 C_2 \int_{-\infty}^{\infty} \int_{-\infty}^{\infty} G(x)\, R(\xi)\, e^{-\frac{ik}{f}[\xi - fx'/D]x}\, dx\, d\xi \quad . \tag{A-18}$$

By geometric lens theory, $D/f = m$, the magnification. If $G(x) = 1$, the first integration yields, using the integral representation of the Dirac δ function

$$W(x') = 2\pi\; C_1 C_2 \int_{-\infty}^{\infty} R(\xi)\, \delta(\xi - \frac{x'}{m})\, d\xi$$

or

$$W(x') = 2\pi\; C_1 C_2\, R(\frac{x'}{m}) \quad .$$

This equation says that the excitation in the object plane at point ξ is proportional to that in the image plane at point $x' = m\xi$; thus the Abbe theory is proved since this is the prediction of single lens theory.

A-VI. ZERNIKE PHASE CONTRAST MICROSCOPY[10]

This mode is based on the Abbe theory of image formation (Appendix A-V). Eq. A-16 may be rewritten as

$$V(x) = C_1 \int_{-\infty}^{\infty} e^{-i\frac{kx\xi}{f}} d\xi + C_1 \int_{-\infty}^{\infty} [R(\xi) - 1] e^{-i\frac{kx\xi}{f}} d\xi \quad . \qquad \text{(A-19)}$$

Here the first term gives the amplitude in the back focal plane in the absence of an object, while the second term is the contribution from the presence of an object. Now in the absence of an object, the radiation is concentrated at the focal point (the intersection of the optic axis with the back focal plane) since an image of the electron source is produced there. This permits the insertion of a filter plate into the back focal plane with a transmission

$$\begin{aligned} G(x) &= e^{i\pi/2} \quad \text{, at source image (first integral of A-19)} \\ &= 1 \quad \text{, elsewhere (second integral of A-19)} \quad . \end{aligned} \qquad \text{(A-20)}$$

Substitution of eqs. A-19 and A-20 into A-17 gives

$$W(x') = C_1 C_2 \left[e^{i\pi/2} + R\left(\frac{x'}{m}\right) - 1 \right] \qquad \text{(A-21)}$$

as seen from eq. A-18 et seq. If the object is a phase object so that $R(\xi) = e^{i\Delta\phi(\xi)}$, and if $\Delta\phi$ is small so that $R(\xi) \simeq 1 + i\Delta\phi(\xi)$, then from eq. A-21, at the image plane

$$I(x') = C \left| e^{i\pi/2} + i\Delta\phi\left(\frac{x'}{m}\right) \right|^2 \simeq C\left[1 + 2\Delta\phi\left(\frac{x'}{m}\right)\right] \qquad \text{(A-22)}$$

where $\xi = \frac{x'}{m}$ and C is a constant.

Thus, if the objective lens is focussed on a weak phase object, with the insertion of a quarter wave plate at the focal point, I(x) becomes proportional to the phase $\Delta\phi(\frac{x'}{m})$.

REFERENCES

1. H. W. Fuller and M. E. Hale, J. Appl. Phys. 31, 238 (1960).

2. H. W. Fuller and M. E. Hale, J. Appl. Phys. 31, 1699 (1960).

3. H. Boersch, H. Raith and D. Wohlleben, Z. f. Physik 159, 388 (1960).

4. H. Boersch, H. Hamisch, K. Grohmann, and D. Wohlleben, Z. f. Physik 167, 72 (1962).

5. H. Boersch, H. Hamisch, D. Wohlleben and K. Grohmann, Z. f. Physik 164, 55 (1961).

6. D. Wohlleben, Physics Letters 22, 564 (1966).

7. D. Wohlleben, J. Appl. Phys. (to be published).

8. L. Marton, J. Appl. Phys. 19, 687 (1948).

9. Y. Aharonov and D. Bohm, Phys. Rev. 115, 485 (1959).

10. M. Born and E. Wolf "Principles of Optics" (Pergamon Press, New York, 1959).

11. H. Jeffries and B. S. Jeffries, "Methods of Mathematical Physics" (Cambridge University Press, 1956), p. 506.

12. H. Nassenstein, Z. angew. Physik 22, 37 (1966).

13. D. Gabor, Proc. Roy Soc. A197, 454 (1949).

14. D. Gabor, Proc. Physical Soc. 64, 449 (1951).

15. J. A. Armstrong, IBM J. Research & Develop. 9, 171 (1965 .

16. W. L. Bragg and G. L. Rogers, Nature, 167, 190 (1951).

17. D. Gabor, G. W. Stroke, D. Brumm, A. Funkhouser, and A. Labeyrie, Nature 208, 1159 (1965).

18. D. B. Dove and P. N. Denbigh, Rev. Sci. Instr. 37, 1687 (1966).

19. H. -D. Dietze and H. Thomas, Z. f. Physik 163, 523 (1961).

20. E. Feldtkeller, Z. angew. Physik 15, 206 (1963).

21. A. Aharoni, J. Appl. Phys. 37, 3271 (1966).

22. J. T. Winthrop and C. R. Worthington, J. Optical Soc. Amer. 56, 588 (1966).

23. D. Gabor and W. P. Goss, J. Optical Soc. Amer. 56, 849 (1966).

24. K. J. Harte, "Spin Wave Effects in the Magnetization Reversal of a Thin Ferromagnetic Film," M.I.T. Lincoln Laboratory Technical Report 364 (August 1964).

25. G. A. Bassett and A. Keller, Phil. Mag. 9, 817 (1964).

26. K. Schaffernicht; Z. angew. Physik 15, 275 (1963).

27. R. H. Wade, Phys. stat. sol. 19, 847 (1967).

28. M. J. Goringe and J. P. Jakubovics, Phil. Mag. 15, 393 (1967).

29. E. Jahnke and F. Emde, Tables of Functions (Dover, New York, 1945).

30. J. Faget, J. Ferre, and C. Fert, Comptes Rendus Acad. Sci. 251, 526 (1960).

31. J. Faget, Revue d'Optique 40, 347 (1961).

32. M. H. Horman, Applied Optics 4, 333 (1965).

33. L. H. Tanner, J. Sci. Instr. 43, 878 (1966).

34. L.O. Heflinger, R. F. Wuerker, and R. E. Brooks, J. Appl. Phys. 37, 642 (1966).

35. R. D. Heidenreich, Fundamentals of Transmission Electron Microscopy (Interscience Publishers, New York, 1964).

36. R. Speidel, Optik 23, 125 (1965).

37. R. Buhl, Z. angew. Physik 13, 232 (1961).

UNCLASSIFIED

Security Classification

DOCUMENT CONTROL DATA – R&D

(Security classification of title, body of abstract and indexing annotation must be entered when the overall report is classified)

1. ORIGINATING ACTIVITY *(Corporate author)*	2a. REPORT SECURITY CLASSIFICATION	
Lincoln Laboratory, M.I.T.	Unclassified	
	2b. GROUP	None

3. REPORT TITLE

Wave Optical Aspects of Lorentz Microscopy

4. DESCRIPTIVE NOTES *(Type of report and inclusive dates)*

Technical Note

5. AUTHOR(S) *(Last name, first name, initial)*

Cohen, Mitchell S.

6. REPORT DATE	7a. TOTAL NO. OF PAGES	7b. NO. OF REFS
10 May 1967	72	37

8a. CONTRACT OR GRANT NO.	9a. ORIGINATOR'S REPORT NUMBER(S)
AF 19(628)-5167	Technical Note 1967-21
b. PROJECT NO. 649L	
c.	9b. OTHER REPORT NO(S) *(Any other numbers that may be assigned this report)*
d.	ESD-TR-67-264

10. AVAILABILITY/LIMITATION NOTICES

Distribution of this document is unlimited.

11. SUPPLEMENTARY NOTES	12. SPONSORING MILITARY ACTIVITY
None	Air Force Systems Command, USAF

13. ABSTRACT

The customary defocussed and Foucault modes of Lorentz microscopy are usually described in terms of geometric optics. Wohlleben has shown that geometric optics has a restricted range of validity, however; a more fundamental approach is provided by wave optics. The defocussed and Foucault modes may be discussed in terms of wave optics, and for the defocussed mode it can be shown explicitly that the geometric theory is simply the first approximation to the wave optics theory. Consideration of wave optics also leads to the proposal of two additional modes of Lorentz microscopy: Zernike phase contrast and interference microscopy; these modes cannot be described on the basis of geometric optics. The most fundamental problems in magnetic films which are amenable to study by Lorentz microscopy are investigations of the fine structures of domain walls and magnetization ripple. These problems are discussed in terms of wave optics for all four modes of Lorentz microscopy; in particular, the intensity distribution of the zero-width divergent domain wall is explicitly calculated for each mode. For practical experiments the importance of coherence, i.e., of the illumination source size, is emphasized, and the experimental aid of holography is suggested. Since the Wohlleben limit is valid for all four modes, however, there is no resolution advantage inherent in any one mode. The choice of modes for solution of the domain wall and ripple problems therefore depends upon experimental convenience. It is concluded that the defocussed mode seems most promising for practical application; Fresnel diffraction is preferred for the domain wall problem, while Fraunhofer diffraction using low angle electron diffraction techniques will be fruitful for the ripple problem.

14. KEY WORDS

microscopy
Lorentz microscopy
geometric optics
wave optics
ferromagnetic films

UNCLASSIFIED

Security Classification

Printed by
United States Air Force
L. G. Hanscom Field
Bedford, Massachusetts